January 2012

Fatigue Behavior Of Continuous Fiber-Reinforced Composite Beams

Mahsud Reimbayev

Fatigue Behavior of Continuous Fiber-Reinforced Composite Beams

by

Mahsud Reimbayev

Bachelor of Science, Turkmen Polytechnic Institute, Turkmenistan, 2003

A Thesis

Submitted to the Graduate Faculty

of the

University of North Dakota

in partial fulfillment of the requirements

for degree of

Master of Science in Mechanical Engineering

Grand Forks, North Dakota

December

2012

This thesis, submitted by Mahsud Reimbayev in partial fulfillment of the requirements for the Degree of Master of Science from the University of North Dakota, has been read by the Faculty Advisory Committee under whom the work has been done and is hereby approved.

_____
Chairperson (Dr. Matthew Cavalli)

_____
Dr. George Bibel

_____
Dr. Marcelin Zahui

This thesis meets the standards for appearance, conforms to the style and format requirements of the Graduate School of the University of North Dakota, and is hereby approved.

_____
Dean of the Graduate School (Dr. Wayne Swisher)

_____
Date

PERMISSION

Title Fatigue Behavior of Continuous Fiber-Reinforced Composite Beams

Department Mechanical Engineering

Degree Master of Science

In presenting this thesis in fulfillment of the requirements for a graduate degree from the University of North Dakota, I agree that the library of this University shall make it freely available for inspection. I further agree that permission for extensive copying for scholarly purposes may be granted by the professor who supervised my thesis work or, in his absence, by the chairperson of the department or the dean of the Graduate School. It is understood that any copying or publication or other use of this thesis or part thereof for financial gain shall not be allowed without my written permission. It is also understood that due recognition shall be given to me and to the University of North Dakota in any scholarly use which may be made of any material in my thesis.

Signature Mahsud Reimbayev

Date 11/29/2012

TABLE OF CONTENTS

LIST OF FIGURES viii

LIST OF TABLES x

AKNOWLEDGEMENTS xii

ABSTRACT xiii

CHAPTER

I. INTRODUCTION. 1

II. BACKGROUND 3

2.1Review of Existing Fatigue Damage Models 3

2.1.1Fatigue Life Models 4

2.1.2 Models Predicting Residual Stiffness or Strength 6

2.1.2.1 Residual Stiffness Models 6

2.1.2.2 Residual Strength Models 8

2.1.3 Progressive Damage Models 11

2.1.3.1 Damage Growth Models 12

2.1.3.2 Damage Growth Models with Residual Mechanical Properties 14

2.2 Models Used in This Study 16

2.2.1 Power Law Model 16

2.2.2 Slaughter's Model 17

2.3 Failure Criteria 20

2.4 Frequency Effect 22

III. MATERIALS, TEST METHODS, EQUIPMENT 24
3.1 Reinforcement 24
3.2 Matrix 26
3.3 Flat Rectangular Plate Construction 27
3.4 Test Specimen Geometries 30
3.4.1 Uniaxial Test Coupons 31
3.4.2 Bending Test Specimens 32
3.5 Static Tests 32
3.5.1 Uniaxial Tests 32
3.5.2 Four-Point Bending Tests 34
3.6 Four-Point Bending Fatigue Tests 35
IV. RESULTS AND DISCUSSION 38
4.1 Static Test Results 38
4.1.1 Uniaxial Test Results of Polyester Resin 38
4.1.2 Uniaxial Test Results of the Composite Material 40
4.1.2.1 Longitudinal Direction 40
4.1.2.2 Transverse Direction 42
4.1.3 Four-Point Bending Tests 45
4.1.3.1 Longitudinal Direction 45
4.1.3.2 Transverse Direction 47
4.2 Finite Element Analysis: ANSYS Results 48
4.3 Stress versus Number of Cycles: Fatigue Test Results 56
4.4 Model Calculation 59
4.4.1 Low Cycle Fatigue Region, Compressive Failure 59
4.4.2 High Cycle Fatigue Region, Tensile Failure 62

4.5 Test Results of Frequency Effect 66

4.6 ANOVA Analysis..... 67

V. CONCLUSIONS AND RECOMMENDATIONS 69

REFERENCES..... 73

LIST OF FIGURES

Figure Page

1. Kink band geometry and notation 17
2. Sinusoidal curves of applied load and response load and deflection 21
3. E-Glass fiber chopped strand mat 24
4. Schematic diagram of VARTM processing 28
5. Schematic of fiber lay-up 30
6. Geometry of tensile test coupons 31
7. Tensile test coupon mounted in the grips of testing machine 33
8. Four-point bending test 34
9. Schematic diagram of load application in four-point bending test 35
10. Four-point bending fixture for fatigue tests 37
11. Polyester resin coupons failed after uniaxial tensile tests 39
12. Stress-strain curves of polyester resin samples in uniaxial tension 39
13. Stress-strain curves of longitudinal E-glass/Polyester composite coupons in uniaxial tension 41
14. Characteristic failure pattern of E-Glass/Polyester composite coupons after uniaxial tensile loading along the fiber direction 42
15. Stress-strain curves of transverse E-Glass/Polyester composite coupons in uniaxial tension 43
16. Characteristic failure pattern of E-Glass/Polyester composite coupons after uniaxial tensile loading in transverse direction 44
17. Stress-strain curves of E-Glass/Polyester composite beams in four-point bending in longitudinal direction 46
18. Typical failure of E-Glass/Polyester composite beams in four-point bending in longitudinal direction 46

19. Stress-strain curves of E-Glass/Polyester composite beams in four-point bending in transverse direction 48

20. Schematic diagram of the loading and constraints of composite beam in ANSYS (Front View)..... 51

21. Schematic diagram of the loading and constraints of composite beam in ANSYS (Isometric View) 51

22. Contour plot of X-component stress corresponding to longitudinal direction 52

23. Failure of E-Glass/Polyester composite beam in pour-point bending in longitudinal direction 53

24. Contour plot of equivalent stress..... 54

25. Contour plot of Y-component stress corresponding to transverse direction 55

26. Contour plot of Z-component stress corresponding to direction through the thickness of the beam 55

27. Contour plot of XZ-component of stress corresponding to interlaminar shear stress of the beam..... 56

28. S-N curve of E-Glass/Polyester composite beam tested in four-point bending fatigue load in longitudinal direction 57

29. Progressive failure pattern of E-Glass/Polyester composite beams tested in four-point bending fatigue load in longitudinal direction 59

30. Slaughter's model predictions with four different parameters compared to experimental data..... 62

31. Log(N_f) variable line fit plot 64

32. Power model prediction compared to experimental data 65

33. Slaughter's model#3 combined with power law model prediction 66

LIST OF TABLES

Table Page

1. Properties of E-glass fibers 25
2. Properties of polyester resin 26
3. Summary of mechanical properties of fibers and resin used in this study 27
4. Volume fraction of 8-layer plates made during the study 29
5. Volume fraction of 2-layer plates made during the study 29
6. Uniaxial test results of resin coupons 38
7. Uniaxial test results of composite coupons in longitudinal direction 40
8. Uniaxial test results of composite coupons in transverse direction 42
9. Four-point bending test results of composite beams in longitudinal direction 45
10. Four-point bending test results of composite beams in transverse direction 47
11. Summary of mechanical properties of composite beam for ANSYS model 49
12. Specimen geometry for ANSYS model 50
13. Summary of ANSYS solution of the composite beam 52
14. Fatigue test results (R=0.1) 57
15. Summary of parameters for Slaughter's model 61
16. Results of calculation of fatigue life using Slaughter's model 61
17. Fatigue test results of composite beam in HCF region used for regression analysis 63
18. Summary of regression analysis 63
19. Fatigue test results of frequency testing 66
20. Fatigue life results for different test frequencies 67

21. Summary of ANOVA analysis from MS Excel 68

22. Results of ANOVA analysis from MS Excel 68

AKNOWLEDGEMENTS

The author wishes to express sincere appreciation to the Department of Mechanical Engineering for their extended long-term support and especially to Professor Matthew Cavalli for his vast reserve of patience and knowledge. This thesis would never have been completed without the encouragement and devotion of my family and friends.

ABSTRACT

A study has been taken to evaluate the fatigue behavior of glass fiber-reinforced composite beams. Due to their highly anisotropic properties, composite beams have different failure modes at different stages of fatigue life. The results of the four-point bending fatigue tests show that the material follows different failure mechanisms depending on the stress level applied to the beam and failure mode changes from compressive failure at high stresses to tensile failure at low stresses. Accordingly, the "stress vs. number of cycles" curve has different slopes at high and low cycle fatigue regions. Two different fatigue damage models, which are used with similar damage mechanisms, were selected. The combination of these two models was applied to composite beam. The methodology of life prediction and calculations are presented. The numerical results are compared to experimental data. The predicted fatigue lives agree with experimental observations very well.

CHAPTER I

INTRODUCTION

The high specific strength and stiffness of fibrous composites make these materials attractive candidates for critical applications in a variety of industries including infrastructure, automotive and aerospace. Many of these applications include cyclic-loading situations, which can degrade the mechanical performance of the materials and generate fatigue failure in the composites. Understanding the fatigue behavior of composite materials is thus of primary importance. Although the fatigue behavior of fiber-reinforced composite materials has been studied for a long time, it is still not possible to make adequate predictions about the fatigue life and degradation of stiffness and strength without extensive special investigation.

Failure of fiber-reinforced composite materials under fatigue loading is more complicated than for metals because of the highly anisotropic characteristics of composites. The anisotropic nature of composites leads to the formation of different stress levels within the material so that the fracture process includes various combinations of damage modes such as matrix cracking, fiber breakage, delamination and ply failure. Voids and defects contained in the composite matrix can act as sites for nucleation of fatigue failure.

Research on fatigue behavior of composite materials is conducted by performing numerous fatigue experiments. Uniaxial tension-tension and tension-compression fatigue are the most preferred ways of working because damage is developing more or

less equally in all layers of composite specimen [1]. Bending fatigue experiments, on the other hand, have been reported by only a few authors [2].

The goal of this research was to evaluate the behavior of fiber-reinforced composite beams under 4-point bending load conditions. Due to high anisotropy of composite materials the fatigue S-N curve of the beam has different slopes in high and low cycle regions. Failure mode of the beam changes from compressive to tensile failure. Compressive failure itself has different mechanisms and it goes from fatigue microbuckling to monotonic microbuckling. Test results show a discontinuous jump in number of cycles as the load increases to a value close to static strength of material. Following principles of beam theory, different predictive models for uniaxial tension and compression loads were evaluated to find a model which would explain fatigue behavior and predict the fatigue life of a composite beam from low to high cycle regions taking into account alterations of failure mechanisms.

CHAPTER II

BACKGROUND

2.1 Review of Existing Fatigue Damage Models

The models used to predict fatigue damage of composites are commonly divided into three major categories: fatigue life models, residual stiffness or strength models and progressive damage models [3].

The fatigue life model does not consider actual damage mechanisms like cracking, fracture or delamination of the material; instead it uses Stress-Life (S-N) curves or Goodman diagrams. Some specific fatigue failure criterion is introduced and fatigue life determined when the criterion is met. Many models have been successfully developed based on well-known S-N diagrams of common materials. However, the behavior of composite materials is essentially different from homogeneous materials.

Residual stiffness models consider the degradation of elastic properties of a specimen. The stiffness is measured frequently during fatigue experiments and the reduction per cycle is analyzed. Deterministic models describe a single-valued property of stiffness, while statistical models predict a stiffness distribution. Some applications require knowledge of the overall strength of the structure and, as a result, the remaining life during which the structure can take a designed load. Therefore, residual strength models have been developed. They describe the degradation of the strength of material during fatigue loading.

Progressive damage models are the third category of predictive models. Their basic concept is that the models for progressive damage are directly related to some specific

damage of the material, such as crack length, delamination or other damage area, etc. The models present some evolution law according to which the measurable damage is developed. Failure occurs when some damage reaches a specified limit [3].

2.1.1 Fatigue Life Models

Fatigue life models take information from S-N curves or Goodman diagrams constructed using experiment data and propose a fatigue failure criterion. They are not based on the damage accumulation but predict the number of cycles at which failure occurs under fixed loading conditions. Examples of fatigue life models are shown below.

Hashin and Rotem's Model

Hashin and Rotem (1973) proposed one of the first fatigue failure criteria in which they distinguished a fiber-failure and a matrix failure mode:

$$\sigma_A = \sigma_A^u \tag{2.1}$$

$$\left(\frac{\sigma_A}{\sigma_T^u}\right)^2 + \left(\frac{\tau}{\tau^u}\right)^2 = 1 \tag{2.2}$$

Where $\sigma_A$and σ_T are the stresses along the fibers and transverse to the fibers, respectively, τ is the shear stress, and σ_A^u, σ_T^u and τ^u are the ultimate tensile, transverse, and shear stresses, respectively. The ultimate strengths are the functions of fatigue stress level, stress ratio and number of cycles. Because of that, the criterion is expressed in terms of three S-N curves which are determined experimentally from testing off axis unidirectional specimens under uniaxial load. This criterion can be used only for laminates with unidirectional plies. Another limitation is that it doesn not allow for multiple possible fatigue failure models [4].

Fawaz and Ellyin's Model

In 1994, Fawaz and Ellyin developed a model introducing a semi-log relationship between applied cyclic stress, S, and the number of cycles to failure, N. They proposed the establishment of a reference S-N line and the determination of two functions:

$$S = m \cdot \log(N) + b \quad (2.3)$$

$$S_r = m_r \cdot \log(N) + b_r \quad (2.4)$$

The second equation applies to the reference line. The relation between the two sets of material parameters (m, b) and (m_r, b_r) is given by:

$$m = f(a_1, a_2, \theta) \cdot g(R) \cdot m_r \quad (2.5)$$

$$b = f(a_1, a_2, \theta) \cdot b_r \quad (2.6)$$

where $a_1$is the first biaxial ratio, $a_2$is the second and R is the stress ratio and θ is an angle of stacking. The general form of the model would be expressed as

$$S(a_1, a_2, \theta, R, N) = f(a_1, a_2, \theta) \cdot [g(R) \cdot \log(N) + b_r] \quad (2.7)$$

The goal of the model is to determine the parameters m and b of a general $S - \log(N_f)$ line for any $a_1, a_2, \theta$and R.The model has shown a good agreement with test results but it is quite sensitive to the choice of reference line, S_r [6].

Bond's Model

In 1999, Bond proposed a semi-empirical model to predict fatigue life for variable loading of glass reinforced composite materials. The relation between applied stress and fatigue life is given by:

$$\sigma_{max} = b \cdot \log(N) + c \quad (2.8)$$

where parameters *b* and *c* are defined as fourth order polynomials of the ratio range, *R".* This function is defined arbitrarily and provides sequential modes of cyclic loading. For example, for tension-tension loading in the Goodman Diagram the R is in the range *0<R<1* and *R"=4+R.* However it is unclear how the relation between R and R" was defined to develop a fatigue model [7].

Xiao's Model

Xiao developed a model to considering the effect of load frequency for thermoplastic carbon/PEEK composite materials. The model predicted fatigue life for *5 Hz* and *10 Hz* using experimental S-N data obtained at *1 Hz.* Xiao constructed a reference S-N curve in the form of power law:

$$p = p_0 + \frac{1 - p_0}{(1 + \tau N)^n} \qquad (2.9)$$

where $p = \sigma/\sigma_u$and $p_0 = \sigma_0/\sigma_u$, in whichσ_u is the static strength and σ_0 is fatigue limit of the material, i.e. a stress level below which no fatigue failure happens. τ and n are defined by curve fitting. The reference temperature was chosen to be$40°C$as it was the maximum temperature during the fatigue testing at *1 Hz* frequency. It was assumed that the isothermal S-N curve at elevated temperature due to hysteretic heating can be determined by shifting the reference S-N curve with two shifting factors, a_T and b_T. Further, an isostrength plot is needed to model the fatigue life prediction under non-isothermal conditions, as the temperature effect associated with hysteretic heating is non-isothermal. These plots can be made by drawing a horizontal line in the $\sigma - \log(N_f)$diagram for a specific stress until it intercepts the isothermal S-N curve. From the area of the hysteretic loop, the heating rate *q* can be calculated and then the temperature rise due to hysteretic heating is determined. The intersection of the temperature curve and iso-strength curve in a $temperature - \log(N_f)$ plot defines the unknown fatigue life [8].

2.1.2 Models Predicting Residual Stiffness or Strength

2.1.2.1 Residual Stiffness Models

Models describing the degradation of elastic properties of composites under fatigue loading are commonly called the residual stiffness models.The variable D is

commonly used to describe the loss of stiffness. In a one-dimensional case it is defined as $D = 1 - \frac{E}{E_0}$ where E_0 is an initial modulus. The residual stiffness and strength models differ from progressive damage models in that they describe the damage growth rate, dD/dN, considering microscopically observable properties, whereas progressive damage models are based on actual damage mechanisms.

Hwang and Han's Model

Hwang and Han in their research established the concept of a fatigue modulus, F. It was defined as the slope of the stress-strain curve of a material at a specific cycle. Then the degradation rate of the fatigue modulus was assumed to be related to the number of cycles to failure through the power function of the form:

$$\frac{dF}{dN} = -AcN^{c-1} \qquad (2.10)$$

where *A* and *c* are the properties of a material. The assumption was made that in any arbitrarily given loading cycle the applied stress, σ_a, varied linearly with resultant strain, so that:

$$\sigma_a = F(N_i) \cdot \varepsilon(N_i) \qquad (2.11)$$

where $F(N_i)$is the fatigue modulus and $\varepsilon(N_i)$is the strain at the loading cycle n_i. After integration and establishing the strain failure criterion, the number of cycles to failure N can be determined as:

$$N = [B(1-r)]^{1/c} \qquad (2.12)$$

where $r = \frac{\sigma_a}{\sigma_u}$ is defined as the ratio of the applied fatigue stress to the static strength. Parameters *B* and *c* are material properties [9].

Sidoroff and Subgio's Model

Sidoroff and Subgio described a damage growth rate model of the form:

$$\frac{dD}{dN} = \begin{cases} \frac{A \cdot (\Delta\varepsilon)^c}{(1-D)^b} & in\ tension \\ 0 & in\ compression \end{cases} \tag{2.13}$$

where $D = 1 - E/E_0, A, b,$ and c are the material parameters that can be determined experimentally. $\Delta\varepsilon$ is the applied strain amplitude. This model was implemented by Van Paepegem and Degrick [10] into a finite element code. Each Gauss-point was assigned a state variable, D, which is related to longitudinal stiffness loss. After calculating one fatigue loading cycle (with the possibility to include inertia and damping forces, contact conditions, friction, etc.), the procedure loops over all Gauss-points and makes an estimate of the value of the local "cycle jump"; this is the number of cycles that can be jumped over without loss of accuracy on the integration of the fatigue evolution law dD/dN for that particular Gauss-point. Finally, the global "cycle jump" for the whole finite element mesh is defined as a certain fraction of the cumulative relative frequency distribution of all local "cycle jump" values. The damage state of the simulated cycle is then extrapolated over the number of cycles that equals the value of the global "cycle jump", after which another fatigue loading cycle is again fully calculated.

The finite element implementation was used to simulate the fatigue behavior of glass fabric/epoxy specimens, which were fatigue loaded as cantilever beams in displacement-control. Due to the different damage distribution through the thickness and along the specimen length, stresses were continuously redistributed during fatigue life. This was accurately simulated by the finite element implementation [11].

2.1.2.2 Residual Strength Models

Residual strength models can be classified into two types: "sudden death" models and "wearout" models. In the low cycle fatigue, when high stresses are applied to a composite material, the residual strength as a function of number of cycles is initially almost constant and suddenly decreases when it is close to the number of cycles to

failure. The “sudden death” model proposed by Chou and Croman [12] describes very well such a condition and it can be successfully used for unidirectional composites of high strength. However, in the region of high cycle fatigue, or the lower stress region, the residual strength of a material degrades more gradually. Such a behavior is well-described by the models commonly called “wearout” models. This type of model is based on the “strength-life equal rank assumption” which states that the strongest material has either the longest fatigue life or the highest residual strength at runout. Hahn and Kim [13] experimentally proved this assumption, but according to Sendeckij [14] it is not necessarily true if different competing failure modes are observed during the fatigue experiments. Also, it cannot always be determined if the models are suitable for both high and low cycle fatigue regions. Usually, researchers do not provide the results of experiments in both regions.

Halpin’s Model

Halpin *et al.* in 1973 initially presented a wearout model which was based on assumption that the residual strength $R(N)$ is a monotonically decreasing function of the number of cycles, N. The change of the residual strength can be described by the power law equation of the form:

$$\frac{dR(N)}{dN} = \frac{-A(\sigma)}{m[R(N)]^{m-1}} \qquad (2.14)$$

where $A(\sigma)$ is a function of maximum cyclic stress and m is a constant [15].

Rotem’s Model

Rotem proposed his model based on the assumption that the initial static strength is maintained up to final fatigue failure. He established an imaginary strength, S_0, in the first loading cycle and assigned to it a value, higher than the static strength. If the S-N curve for tension-tension fatigue is given by:

$$S = 1 + K \cdot \log(N) \qquad (2.15)$$

where $S = \frac{S_f}{S_0}$ in which S_f is the fatigue strength for constant amplitude and S_0 is the imaginary strength, then the fatigue life that remains after a certain number of loading cycles can be determined by a curve resembling the S-N curve but with different slope, which passes the S_0. This curve is called a damage line and the family of such damage lines is defined by:

$$S = 1 + k \cdot \log(N) \qquad k < K \qquad (2.16)$$

As long as the degradation of residuals strength pertains to the interval between imaginary strength and static strength, no apparent degradation of the strength is observed. In 1991, Rotem extended the cumulative fatigue theory based on these assumptions to use it for composite laminates under cyclic loading with arbitrary but constant stress ratio [16].

Caprino and D'Amore's Model

In 1998, Caprino and D'Amore carried out four-point bending fatigue experiments and studied the fatigue behavior of a random continuous-fiber-reinforced thermoplastic [ref]. The damage model that they proposed was based on the assumption that the residual strength decays continuously and the damage process follows a power law of the form:

$$\frac{d\sigma_n}{dn} = -a_0 \cdot \Delta\sigma \cdot n^{-b} \qquad (2.17)$$

where σ_n is the residual strength after *n* cycles, $\Delta\sigma = \sigma_{max} - \sigma_{min}$ the parameter that considers the influence of the stress ratio R, a_0 and b are constants for a material. The goal of Caprino and D'Amore was to develop a model which would take into account the effects of both the stress ratio and different behavior of a material on the regions of low and high cycle fatigue. They observed a change in a failure mode from matrix shear yielding at low cycle fatigue (high applied stress) to a single crack growth at high cycle

fatigue (or low applied stress). Also, Caprino and D'Amore found that the higher the material sensitivity to stress amplitude, the lower the sensitivity to the number of cycles. This means that conclusions made on observations of fatigue behavior on the low-cycle fatigue region are not necessarily the same as those made on high-cycle fatigue region. Later, Caprino and Giorleo successfully applied the model to four-point bending fatigue of glass-fabric/epoxy composite materials [17].

In 2000, Caprino tried to apply the residual strength model to carbon fiber-reinforced composites under tension-tension fatigue loading condition. He came to conclusion that the model is able to predict the fatigue life of the material but the experimentally measured residual strength is not in agreement with that determined by the residual strength law. Therefore, in a case of tension-tension fatigue the model can be used but it becomes a fatigue life model rather than a residual strength model [18].

2.1.3 Progressive damage models

The major difference between progressive damage models and those described above is that progressive damage models establish one or more properly chosen damage variables. These variables define the degradation of composite material. Such models reflect the actual physical processes that stand behind the damage mechanisms which lead to the microscopically observable degradation of the mechanical properties of a material. Generally, the models are divided into two classes: the damage models which predict the growth of the damage such as the number of transverse matrix cracks per unit length, size of the delamination area, etc., and another class is the models which correlate the damage growth with the residual mechanical properties (stiffness/strength).

2.1.3.1 Damage Growth Models

Several models have been proposed to represent the damage accumulation for a certain damage type, such as matrix cracks or delamination, and typically they make use of experiments on notched specimens to initiate a specific damage type at a well-known site [ref].

Biner and Yuhas's Model

In 1989, Biner and Yuhas studied the growth of fatigue cracks in woven glass/epoxy composite materials. They showed that the initiation and growth rate of small cracks originating from blunt notches can be described by ΔK_{eff}, the range of effective stress intensity factor. Considering the notch and crack geometry, ΔK_{eff}, was determined using conformal mapping methods. Further, when the crack length was long enough it was converged to ΔK [19].

Dahlen and Springer's Model

Dahlen and Springer developed a semi-empirical model to estimate the delamination growth in graphite/epoxy composites under fatigue loading. The model included Mode I, Mode II and mixed-mode conditions. The contribution of Mode III on the delamination growth was considered to be insignificant. Also, viscoelastic and thermal effects were assumed to have negligible effect.

The crack growth rate was given to be of similar form to the Paris Law:

$$\Delta a \frac{\sigma_f^2}{E_y G_{crit}} = A\left(U \frac{G_{max}}{G_{crit}}\right)^b \qquad (2.18)$$

where Δa is the growth of delamination normal to the circumference of the existing delamination, σ_f is the strength of the ply in transverse direction, E_y is modulus of elasticity of the ply in transverse direction, G_{crit} is the critical energy release rate (which has contributions from both Mode I and Mode II), *A* and b are material constants and

also depend on the relative contribution of the Mode I and II to the growth of delamination, and U is a function of G_{max}/G_{crit} and G_{min}/G_{max}. G_{max} is the maximum energy release rate during one cycle. In order to evaluate the model three types of tests were conducted on graphite/epoxy composites under mode I, Mode II, and mixed mode conditions using double cantilever beam, end notched cantilever beam and mixed mode bending test coupons. The delamination growth rate results measured during the tests and determined by the model were found to be in a good agreement [20].

Feng's Model

Feng *et al.* proposed a model which predicts fatigue damage growth in carbon fiber reinforced composited due to matrix cracking. Based on experiments that they observed, they came to a conclusion that Mode I crack growth rate can be described by Paris Law of the form:

$$\frac{dS}{dN} = A\left(\frac{G_I}{G_{max}}\right)^n \tag{2.19}$$

where A is the damage area of the matrix cracking, N is the number of cycles, G_{max} is the maximum energy release rate in one cycle, D and n are the parameters of a material. The value of G_{max} is determined using finite element calculations. Finite element analysis of the local region is run iteratively to simulate the growth of the damage. Such a method allows the relation between A and G_{max} to be determined. When the fiber strain exceeds the fiber fracture strain, fatigue failure occurs. In such a way the fatigue life, N_f, and the final damage area A_f are determined.

Experimental results on an I beam tested under four-point bending fatigue load and on a notched coupon under tensile fatigue loading were compared to model predictions and good agreement was found between the damage area measured during the tests and determined by the model [21].

2.1.3.2 Damage growth models with the residual mechanical properties

This type of damage model is based on the relation of the damage variable with the residual mechanical properties, such as stiffness or strength of the material. The damage growth rate is generally based on damage mechanics, thermodynamics, micromechanical failure criteria or some certain damage characteristics such as crack spacing, area of delamination, etc.

Ogin's Model

In 1985, Ogin *et al.* proposed a simple relation that described the stiffness reduction for $(0/90)_s$ glass fiber-reinforced laminate:

$$E = E_0(1 - cD) \tag{2.20}$$

where $D = 1/2s$ is the average crack density, $2s$ is the average crack spacing and c is a material constant. E_0 is the initial stiffness of a material. They assumed that the crack growth rate is a power function of the stored elastic energy between two neighboring cracks in the transverse ply. Using equation *2.20*, the stiffness degradation rate was derived and had a following form:

$$-\frac{1}{E_0} \cdot \frac{dE}{dN} = A\left[\frac{\sigma_{max}^2}{E_0^2\left(1 - \frac{E}{E_0}\right)}\right]^n \tag{2.21}$$

where $\sigma_{max}$is the applied fatigue stress, A and n are the material properties.

In 1987-1990, Beaumont used equation 2.*21* to determine S-N curves by applying the strain failure criterion and specifying D_f as the critical value of the damage variable, D.

If the delamination was the dominating damage mechanism, Beaumont specified the damage variable, D, as:

$$D = \frac{A}{A_0} = 2.857\left(1 - \frac{E}{E_0}\right) \tag{2.22}$$

where A is the area of delamination and $A_0$the total area between plies [22].

In 1988, Carswell presented a model for laminates with unidirectional plies. The damage variable, D, is based on the length of the matrix crack in the laminate. The form of the model was as follows:

$$\frac{dD}{dN} = p\sigma_c \frac{D^2}{N} \qquad (2.23)$$

where p is a constant, σ_c is the fatigue stress and D is the value related to the stiffness and given by equation *2.20* [23].

Caron and Ehrlacher's Model

Caron and Ehrlacher presented a model that describes the fatigue microcracking process in cross-ply laminates. The model is based on the idea of discretization of 90° plies into sections where cracking is more preferable. The strength in these sections is randomly distributed. The propagation of the crack is assumed to follow the Paris Law and the residual strength degradation of the material follows an equation of the form:

$$\frac{dRe}{dN} = -CRe^{3-\eta}\Delta S^{\eta} \qquad (2.24)$$

where Re is the residual strength,C and η are material properties and ΔS is the stress range. The residual life is determined from this equation and then, by iteration, the stress in each section is calculated and compared with the residual strength. If the section breaks, then stresses are redistributed and the residual life of each section is calculated [24].

Presented above are only a few examples of fatigue damage models developed to predict life of composite materials. More detailed information about major fatigue damage models and life prediction methodologies that have been successfully used among researchers can be found in the Degrieck and Van Paepegem's review of damage modeling [3].

2.2 Models Used in This Study

Two different models were used in this study to describe the constitutive behavior of composite beams because the observed failure mode changes from tensile to compressive failure as the applied stress increases. Only tensile failure was observed in the high cycle fatigue (HCF) region which corresponds to fatigue life from around 20 thousand cycles to 2-3 million cycles and relatively low applied stress levels. In the low cycle fatigue (LCF) region (high applied stress level) compressive failure dominated. A distinct transition from tensile to compressive failure was clearly seen on the S-N curve as a change of a slope of the curve.

2.2.1 Power Law Model

S–N behavior of FRP laminates in the HFC region has been described by the wear-out model by Sendeckyj [13] as a power curve. It is similar to Basquin's relation of the form:

$$S = AN_f^n \qquad (2.26)$$

where A and n are material constants and can be determined from experimental data.

The fatigue behavior in the LCF region where compressive failure dominates was well described by Slaughter and Fleck [25]. Analyzing the compressive behavior of composite materials, they justified the existence of a plastic collapse point where the slope of S-N curve suddenly changes. In fact, in the LCF region, where compressive failure dominated, the test results of composite beams showed a sudden jump in fatigue life when stress was increased to the level close to static strength of material. Slaughter's model for compressive behavior of FRC was in a good agreement with our test results of glass-fiber composite beams.

2.2.2 Slaughter's Model

W. S. Slaughter and N. A. Fleck analyzed compressive fatigue of fiber composites and presented a fatigue model based on micro-buckling under monotonic loading developed earlier by Budiansky and Fleck [26]. Micro-buckling is a phenomenon in which localized deformation occurs within a kink band. This kink band, in general, is not normal to the fiber direction and forms an angle β with a direction normal to the fibers and has a width, ω. The kink band was modeled as in Fig 1.

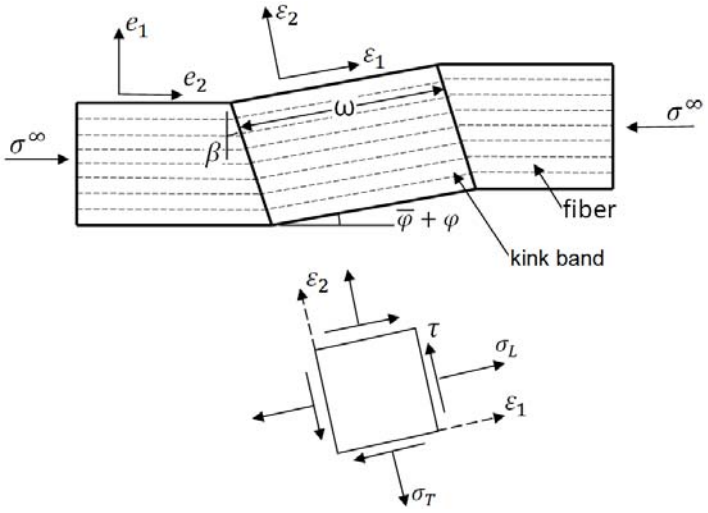

Fig.1 Kink band geometry and notation

It was assumed that the fibers are inextensible and deformation was given by the fiber rotation, φ. It was also assumed that the initial composite fiber misalignment can by approximated by an initial kink band fiber rotation, $\overline{\varphi}$. Budiansky and Fleck [26] derived an expression for kinematic conditions and continuity of tractions across the kink band interface:

$$\sigma^\infty \cos\beta \sin(\overline{\varphi}+\varphi) = \tau \cos(\beta - \overline{\varphi} - \varphi) + \sigma_T \sin(\beta - \overline{\varphi} - \varphi) \quad (2.27)$$

where σ^∞ is a remote compression, σ_T, τ -transverse and shear stresses within kink band, respectively, $\overline{\varphi}$-initial fiber misalignment, φ-fiber deformation, β-angle between kink band and direction normal to fibers. Considering that small values of φ will be

sufficient to describe the microbuckling phenomenon, eq.*2.27* above can be reduced to approximate equilibrium:

$$\sigma^{\infty} \approx \frac{\tau + \sigma_T \tan\beta}{\overline{\varphi} + \varphi} \tag{2.28}$$

Slaughter and Fleck re-wrote the equilibrium equation *2.27* in terms of effective shear stress, τ_e, and strain, γ_e. Defining the pure shear yield strain as $\gamma_y = \tau_y/G$, equation *2.27* was rewritten as:

$$S^{\infty} = \frac{t}{\overline{\omega} + \eta} \tag{2.29}$$

where $S^{\infty} = \sigma^{\infty}/G^*$, $t = \tau_e/\tau_y$, $\eta = \gamma_e/\gamma_y$ and $\overline{\omega} = \overline{\varphi}/\gamma_y^*$ are non-dimensional variables.

$$\begin{cases} G^* = \alpha^2 G \\ \gamma_y^* = \gamma_y/\alpha \end{cases} \tag{2.30}$$

Parameter α defines relation between effective strain, y_e, and fiber rotation, φ, in a function:

$$y_e = \alpha\varphi \tag{2.31}$$

where

$$\alpha = \sqrt{1 + R^2 tan^2\beta} \tag{2.32}$$

In which R defines the eccentricity of the yield ellipse and equal to:

$$R = \frac{\sigma_{Ty}}{\tau_y} \tag{2.33}$$

where σ_{Ty}, τ_y are transverse and shear yield stresses, respectively.

Representing equilibrium *2.29* on a Considere Diagram, Budiansky and Fleck have shown that, for a Ramberg-Osgood composite material response, the micro buckling solution has a form:

$$\left.\begin{aligned} t_c &= \left[\frac{7\bar{\omega}}{3(n-1)}\right]^{1/n} \\ S_c^{\infty} &= \frac{1}{1+n\left(\frac{3}{7}\right)^{1/n}\left(\frac{\bar{\omega}}{n-1}\right)^{(n-1)/n}} \end{aligned}\right\} \qquad (2.34)$$

where *n* is a material parameter, and t_c and S_c^{∞} are parameters representing critical strain and stress, respectively. This form of Considere Diagram was utilized in the analysis of local kink band response to remote cyclic compressive loading. As a result of the analysis, the effective plastic strain experienced by the kink band during compressive fatigue loading was found to be:

$$\Delta\eta = \frac{6}{7}(\Delta t/2)^n \qquad (2.35)$$

where $\Delta\eta$ and Δt are changes in effective plastic strain and stress, respectively. n is the material parameter.

In order to obtain $\Delta\eta^p$ as a function of s_{max}^{∞}, s_{min}^{∞}, $\bar{\omega}$ and *n*, the following equations are solved:

$$t_2 - S_{max}^{\infty}\left(t_2 + \frac{3}{7}t_2^n + \bar{\omega}\right) = 0 \qquad (2.36)$$

$$\Delta t - \left(1 - \frac{S_{min}^{\infty}}{S_{max}^{\infty}}\right)t_2 + S_{min}^{\infty}\left(\Delta t + \frac{6}{7}(\Delta t)^n + \bar{\omega}\right) = 0 \qquad (2.37)$$

First eq.*2.36* is solved for t_2. It has n solutions but the smallest positive real solution is the one of interest. Then eq.*2.37* is solved for Δt. Finally, the effective plastic strain, $\Delta\eta$, can be found by substituting Δt in eq.(2.35). Once the effective plastic strain is determined then a Coffin-Manson type fatigue relationship is used to find the number of cycles to failure:

$$\frac{\Delta\eta}{2} = \frac{\gamma_f'}{y_y}(2N_f)^c \qquad (2.38)$$

where γ_f' and $c$are material parameters.

The upper limit of cyclic loading is given by:

$$S^{\infty} < (1-\rho)S_c^{\infty} \tag{2.39}$$

where S_c^{∞} is a parameter related to the monotonic microbuckling load or the compressive strength of composite material. As the applied load increases, the failure mode changes from fatigue to monotonic microbuckling. The monotonic microbuckling is represented by a horizontal line:

$$S^{\infty} = (1-\rho)S_c^{\infty} \tag{2.40}$$

The transition generally does not occur at $N_f = 1$. Fatigue microbuckling is the process defined by Coffin-Manson relation *2.35* as a result of the kink band analysis. The model predicts an abrupt change of the slope of S-N curve as the applied force increases. Slaughter and Fleck's research shows that there is a strong dependence of fatigue life on the Ramberg-Osgood parameter, n, and the Coffin-Manson composite parameter, c, and a much weaker dependence on γ_f'. Typically the values for n are in a range of 2 - 5 and for *c* they are in a range of -0.5 - -0.7 for unidirectional fiber composites [25].

2.3 Failure Criteria

There are several ways to define failure. The most obvious is when complete separation or fracture occurs. More generally, failure occurs when a component can no longer fulfill the function for which it was designed. This definition includes not only total fracture, but also large deformations like buckling or delamination.

In the case of a bending unidirectional composite beam, according to beam theory, the outer layers experience the highest stress, so they are damaged first. Once failure occurs in the outer layer its stiffness and strength decrease to zero. The beam acts the like a beam with a new thickness and stiffness. Damage progresses gradually from the outer layer to inner layers until the whole structure collapses. For such a behavior, a damage degradation model would be appropriate. However in practice it was

found that after failure of outer layers the beam loses its stability. Even though the whole structure still looks stiff and strong, an uneven damage of the surface causes unstable response to applied load. This is clearly seen on the sinusoidal response curve of load or deflection during a fatigue test. Figure 2 is the screenshot taken during a fatigue test when the specimen was just about to fail. The red sinusoidal curve corresponds to applied load while blue and green curves represent the unstable load and deflection response of a specimen.

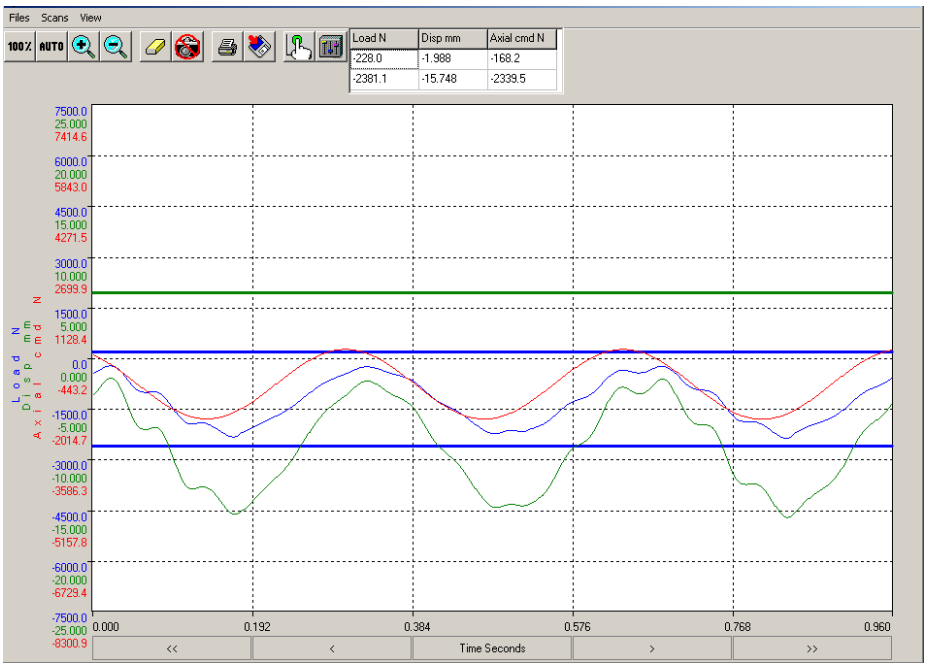

Fig.2 Sinusoidal curves of applied load and response load and deflection

At some point, such a response creates resonance with the applied load which leads to overloads, which, in turn, stops the testing machine. Further testing of the same specimen was impossible. After such a failure, i.e. automatic stop of machine due to resonance, inspection of specimens showed that all of them had identical failure mode: complete failure of first layer with little or no propagation to the second layer of the composite beam. Thus, we decided to test specimens until first ply failure and the machine stopped due to resonance overloads.

2.4 Frequency Effect

Fatigue tests are undertaken normally at the highest frequency possible in order to minimize the time and cost of undertaking a fatigue program. Effects of frequency on fatigue life have been studied for many types of fiber composites with the following areas of concern: hysteretic heating, rate of damage generation and strain rate effects on the residual strength on the last cycle [28].

Considerable hysteretic heating effects were noticed in high test frequencies ranging from 20 Hz to 100 Hz. Increasing test frequency caused heating which, in turn, decreased the fatigue life of a composite material. Frequency levels below 20 Hz did not show a significant temperature rise [27].

Frequency effects other than from hysteretic heating are small [28]. Glass fibers and polymeric matrices can show significant effects of constant load (static) fatigue, and it has been shown that time at maximum load causes much higher damage than the strain rate used in reaching that load [29,30]. However, fatigue behavior tends to be most influenced by the number of cycles, not the frequency of cycling, particularly at high cycles [29,30]. In the latest fatigue standard on fiber reinforced plastic composites published, ISO 13003, it is recommended to keep the frequency in a range from 1Hz to 25 Hz in order to keep the temperature rise of composite material at an acceptable level [31]. The test frequency in the current study varied from 3 Hz to 8 Hz depending on the applied load. This level is well below the frequency levels which can cause considerable heating. The frequency needed to be varied somewhat to maintain specimen stability under different loading conditions. For some stresses resonance would occur. To check that change in frequency level did not significantly affect the test results, i.e. fatigue strength and life, a statistical analysis was performed using ANOVA statistical tool. Several tests under the same stress level but different test frequencies were run and

statistical significance of the results was evaluated. The results of the analysis are presented later in this paper.

CHAPTER III

MATERIALS, TEST METHODS, EQUIPMENT

3.1 Reinforcement

In this study, the reinforcement material used for specimen fabrication was unidirectional E-glass-fiber stitch-bound to chopped strand mat. The material was supplied by LM Wind Power, a company manufacturing wind turbine rotor blades. Most rotor blades are constructed using mainly this glass-fiber reinforcement. It is unidirectional fabric, with some strands that are woven in the transverse direction. One side of the fabric is covered with glass-fiber chopped strands. Portion of fibers in transverse direction together with chopped strands was found to be less than 6% by weight. It was determined by separating chopped strands and transverse fibers from original fabric and measuring the weight of the material before and after separation. Fabric architecture is shown in Fig.3.

Fig.3 E-glass fiber chopped strand mat

Properties of this particular material were not available, but general properties of E-glass are listed in Table 1:

Table 1 Properties of E-glass fibers [35]

Fiber Material	E-glass
Tensile Strength (MPa)	1700-3500
Density (g/cm^3)	2.49
Modulus (GPa)	73
Shear Modulus (GPa)	30
Poisson's Ratio	0.23
Density (g/cm^3)	2.49

These properties were verified for the reinforcement used in this work as detailed below. According to the rule of mixtures the elastic modulus of a unidirectional composite beam tested in longitudinal direction is given by:

$$E_1 = v_f \cdot E_{1f} + v_m \cdot E_m \qquad (3.1)$$

where E_1 is elastic modulus of composite in longitudinal direction, E_{1f} and E_m are elastic modules of fibers and matrix and v_f, v_m are volume fraction of fibers and matrix, respectively.

$E_1 = 36.2\ GPa, E_m = 2.9GPa, v_f = 0.50$ (determined experimentally-see chapter 4.2.1)

From eq.*3.1*

$$E_{1f} = \frac{E_1 - E_m \cdot v_m}{v_f} \qquad (3.2)$$

$$E_{1f} = \frac{36.2 - 2.9 \cdot 0.50}{0.50} = 69.5\ GPa$$

The strength of fibers can be estimated in the same way:

$$F_1 = v_f \cdot F_f + v_m \cdot F_m \qquad (3.3)$$

where F_1 is strength of composite material, F_f and F_m are strengths of fibers and matrix, respectively.

$F_1 = 920\ MPa, F_m = 50\ MPa$ (see chapter 4)

From eq.*3.3*

$$F_f = \frac{F_1 - F_m \cdot v_m}{v_f} \tag{3.4}$$

$$F_f = \frac{920 - 50 \cdot 0.50}{0.50} = 1790\ MPa$$

3.2 Matrix

The resin used to fabricate the test samples was polyester resin, **POLYLITE® 413-575** supplied by **REICHHOLD Inc.** Basic properties of polyester resins are generally known and shown in Table 2:

Table 2 Properties of polyester resin [35]

Resin Type	Polyester
Tensile Strength (MPa)	40-90
Compressive Strength (MPa)	90-250
Shear strength (MPa)	45
Elastic Modulus (GPa)	3.2-3.5
Shear Modulus (GPa)	0.7-2.0
Poisson's Ratio	0.3-0.35
Density, g/cm^3	1.1-1.5

In order to obtain the mechanical properties of the resin used, several test coupons were made from pure resin and tested uniaxially following ASTM D3039 [36].

According to test results (see ch.4) the average modulus of elasticity of the resin is

$E_m = 2.9\ GPa$

The resin shear modulus was calculated, assuming that the Poison's ratio of the resin $\nu = 0.35$:

$$G_m = \frac{E_m}{2 \cdot (1 + 0.35)} \tag{3.5}$$

$$G_m = \frac{2.9}{2 \cdot (1 + 0.35)} = 1.074\ GPa$$

The average resin tensile strength was determined from uniaxial tests (see ch.4) to be $F_m = 50\ MPa$

Table 3 is the summary of mechanical properties of the reinforcement and matrix materials, which were used for further calculations in this study:

Table 3 Summary of mechanical properties of fibers and resin used in this study

Component	Reinforcement	Matrix
Material Type	E-Glass	Polyester Resin
Elastic Modulus (GPa)	69.5	2.9
Shear Modulus (GPa)	30.0	1.074
Tensile Strength (MPa)	1790	50
Poisson's Ratio	0.23	0.35

3.3 Flat Rectangular Plate Construction

Initially, the specimens for this study were made using hand lay-up manufacturing process. But the desired consistency in properties of the test specimens could not be achieved. There was too much variation in fiber volume fraction, density, thickness of specimens, presence of pores, etc. The manufacturing method was then changed to vacuum assisted resin transfer molding (VARTM) which significantly improved the quality and, more importantly, the consistency of properties of the test specimens. The standard deviation of volume fraction of the specimens made by VARTM process was *1.5%* of the average value and the standard deviation of the thickness was less than *0.5%* of the average thickness.

VARTM is a variant of the traditional resin transfer molding (RTM) process. In VARTM, the upper half of a conventional mold is replaced by vacuum film. When vacuum is created between the rigid mold surface and the film over the fibers, the outer atmospheric pressure compresses the fibers. In this way, the thickness of the final

material is determined only by the thickness of the fibers. Thus, for the same type of fibers and number of plies the final thickness is relatively constant. Fig.4 is a schematic diagram of the VARTM lay-up.

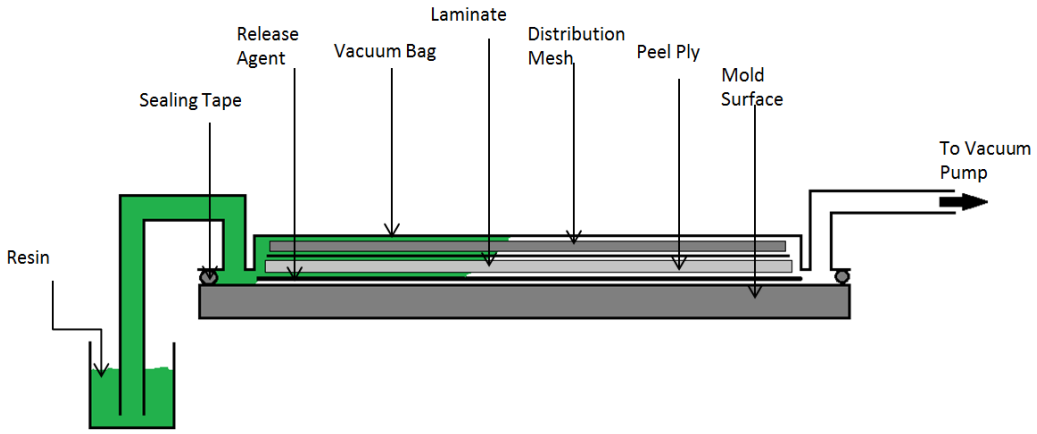

Fig.4 Schematic diagram of VARTM processing

First, a rigid work surface is covered with a thin layer of release agent and the necessary number of dry fiber fabric plies is placed. The stacked reinforcement is covered with a combination of materials to promote the resin flow and provide the easy removal of the laminate. Normally, the top layers include a peel ply fabric and resin distribution mesh. The mesh provides a better resin flow over the surface of the laminate. The peel ply provides easy removal of the layer of the mesh and uniform resin saturation through itself to the laminate. Lines of resin feed are positioned over the resin flow mesh. This includes the tubing for resin supply and air removal and spiral tubes for uniform distribution of the resin. The entire assembly is then covered by vacuum film and then the vacuum pump is turned on to expel air from the cavity between rigid surface and the top film. After the system has been equilibrated and all the air leaks are eliminated, the resin is allowed to flow into the laminate. The vacuum is left on until the resin has completely gelled. The part may then be cured at room temperature or in an oven.

Table 4 lists the values of the average volume fraction and thickness of the 8 layer plates made for fatigue and static bending tests. All the values were determined by the burn off test according to ASTM D3171 [37].

Table 4 Volume fraction of 8-Layer plates made during the study

Plate #	Average V_f (%)	Average Thickness (mm)
PB 1	59.9	6.45
PB 2	58.8	6.40
PB 3	58.1	6.35
PB 4	58.0	6.58
PB 5	58.0	6.34
PB 6	57.3	6.59
PB 7	59.7	6.25
PB 8	60.2	6.57
PB 9	59.5	6.35
PB 10	58.8	6.40
PB 11	59.4	6.45
PB 12	59.5	6.40
Average	58.9	6.43
STDV	0.91	0.11

The plates for uniaxial tensile tests had 2 layers. The volume fraction of fibers of tensile coupons is given in Table 5.

Table 5 Volume fraction of 2-layer plates made during the study

Plate #	Average V_f (%)	Average Thickness (mm)
PU 1	53.9	1.80
PU 2	53.4	1.80
Average	53.7	1.80
STDV	0.35	0.00

The volume fraction of tensile specimens in average was *53.7%*. For calculation purposes it was considered as *50%*. The reason is that about *6%* of fibers by weight in the glass fabric were in transverse direction and practically did not contribute for tensile strength of the material $53.7 - 53.7 * 0.06 \approx 50\%$

3.4 Test Specimen Geometries

All specimens were manufactured in 1x1 ft. flat plates in a vacuum assisted resin transfer molding (VARTM) process. The polyester resin was mixed with 1.5% of MEKP (catalyst). The panel was cured using the manufacturer's recommended cure cycle. In this case, it was a 16 hour hold at temperature of *45* ℃. For uniaxial tests, 2 layers of glass fabric were used and the resulting plate thickness was *1.8* mm. For 4-point bending tests, 8 layers of glass fabric were used and plate thickness was *6.43* mm. The average fiber volume fraction for uniaxial specimens was *53%* and for bending tests was *59%.* One side of fabric was covered by chopped strands, so in order to keep symmetry about the neutral plane of the beam, 4 plies were placed with chopped strands down and another four were placed with chopped strands up. Here two compositions were possible. Chopped strands face to each other or clean sides face to each other in a midplane. When chops faced each other some specimens failed by shear mode during 4 point bending test. But no shear failure was observed when clean sides of fabric were faced to each other. The decision was made to put the clean surface of the fabric facing each other to keep symmetry about the neutral plane of the beam. In a Figure 5 the fiber lay-up is shown schematically.

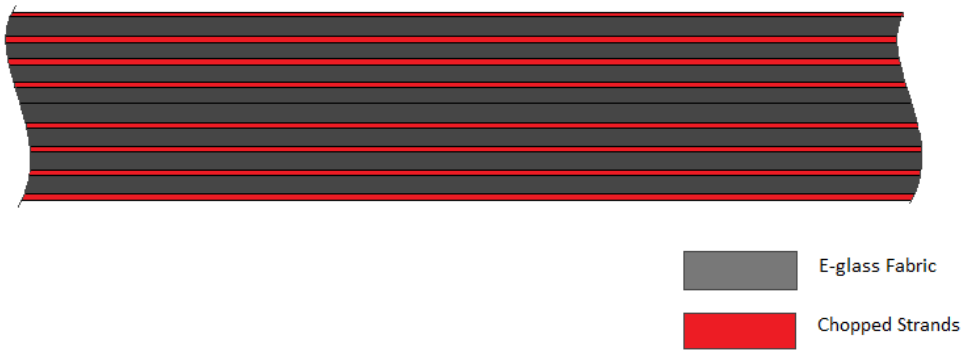

Fig.5 Schematic of fiber lay-up

3.4.1 Uniaxial Test Coupons

Uniaxial test plates were cut into coupons using a diamond saw. Details about coupon geometries are given in ASTM specification D3039 [36]. The longitudinal (0°) coupons were made *12.7* mm wide, while transverse (90°) coupons were *25.4 mm* wide. The geometries of uniaxial tensile specimens are depicted in Figure 6.

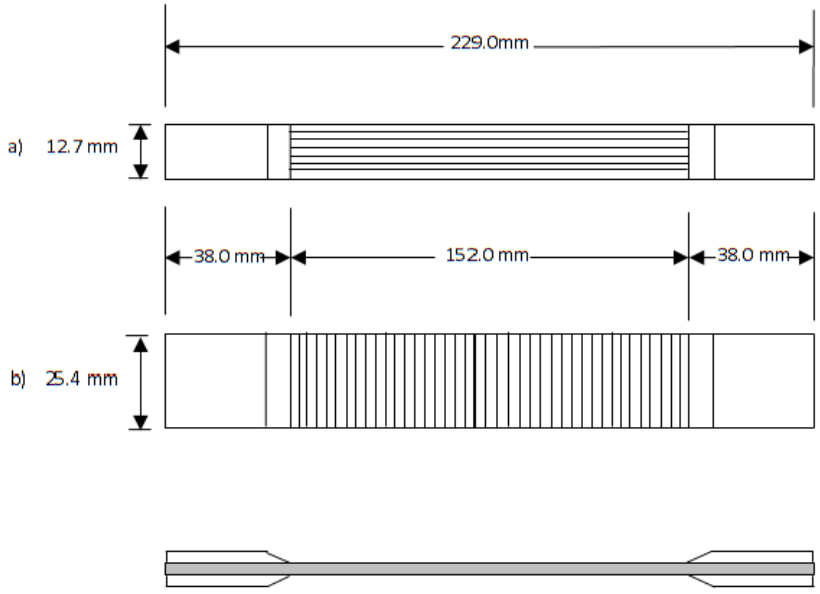

Fig.6 Geometry of tensile test coupons

a) Longitudinal tensile [0º]
b) Transverse tensile [90º]

Tab material was bonded to the tensile coupons to avoid material damage while fixed in the steel wedge grips. The tabs were made from steel and bonded using Aralldite 2000 industrial glue which was found to be the best in this particular application. One change was made in tab size. When the first few longitudinal coupons were tested,

some damage of the material was observed on the edges of tabs. The width of the tab did not cover fully the composite and material on the side was sort of loose. Because of that, the tabs were made little wider to make sure that tabs, together with the glue, fully enfold the composite material. In this way the damage on the sides was prevented and the highest composite strength was achieved.

3.4.2 Bending Test Specimens

For both static and fatigue bending tests coupons were identical. Plates were cut into specimens using a diamond saw to cut in the longitudinal direction, and an 80-tooth saw blade to cut in the transverse direction of the fibers. This was done because when the diamond saw was used to cut in transverse direction it created overheating of the material and melted the resin on the edges. The 80-tooth saw blade gave a very good surface finish. The 80 teeth saw was not suitable to cut in the longitudinal direction because the rare transverse fibers were not cut but ripped which created micro cracks which would create stress concentrations during fatigue tests. The average thickness of coupons was *6.43* mm and the average width was *25.4* mm. The load span was *203.2* mm for all bending tests, so the length of the specimens was about *250* mm. Both longitudinal and transverse bending test specimens had the same geometry.

3.5 Static Tests

All static tests were performed using a SHIMADZU AG-IS testing machine. The maximum load capacity of the machine is 50 kN.

3.5.1 Uniaxial Tests

All uniaxial tests were performed according to ASTM D3039 [36]. This standard method determines the in-plane tensile properties of polymer matrix composite materials reinforced by high modulus fibers. The test coupon was mounted in the grips of the universal testing machine and monotonically loaded in tension at a rate of 2 mm/min. In

the middle of the coupon an electronic extensometer with *25 mm* gage length was mounted (see Fig.7).

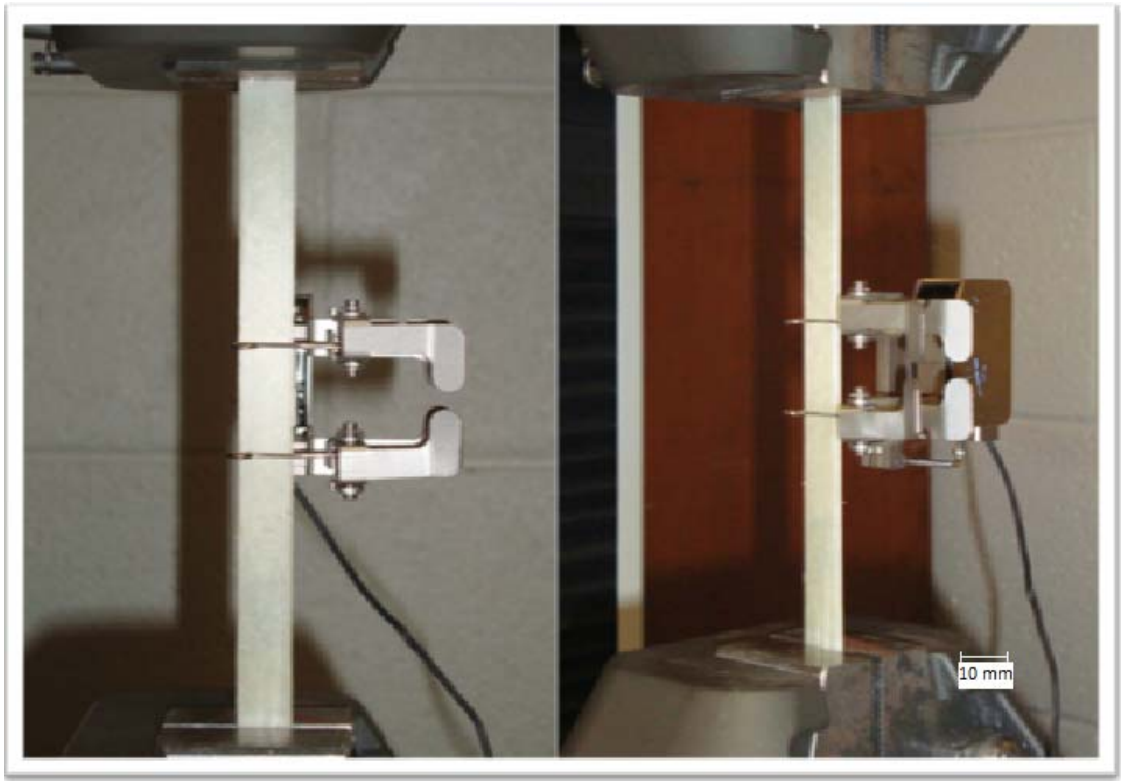

Fig.7 Tensile test coupon mounted in the grips of testing machine

All the tests were performed at ambient temperature.

Both load and displacement were monitored and recorded. The stress-strain response of the specimen was used to determine the ultimate tensile strength and tensile modulus of elasticity.

The stress at each required data point was calculated using equation:

$$S = \frac{P}{A} \qquad (3.6)$$

where S – tensile stress [*MPa*], P – applied load [*N*], A – average cross-sectional area [mm^2]

Tensile strain was calculated as:

$$\varepsilon = \frac{\delta}{L_g} \tag{3.7}$$

where ε - tensile strain [*mm/mm*], δ - extensometer displacement at a given data point [*mm*], L_g - extensometer gage length [*mm*].

3.5.2 Four-Point Bending Tests

The bending tests were performed following ASTM D6272 [38]. This test method is used for determination of flexural properties of unreinforced and reinforced plastics, including high modulus composites. A bar of rectangular cross section rests on two supports and is loaded at two points (by means of two loading noses), each an equal distance from the adjacent support point.

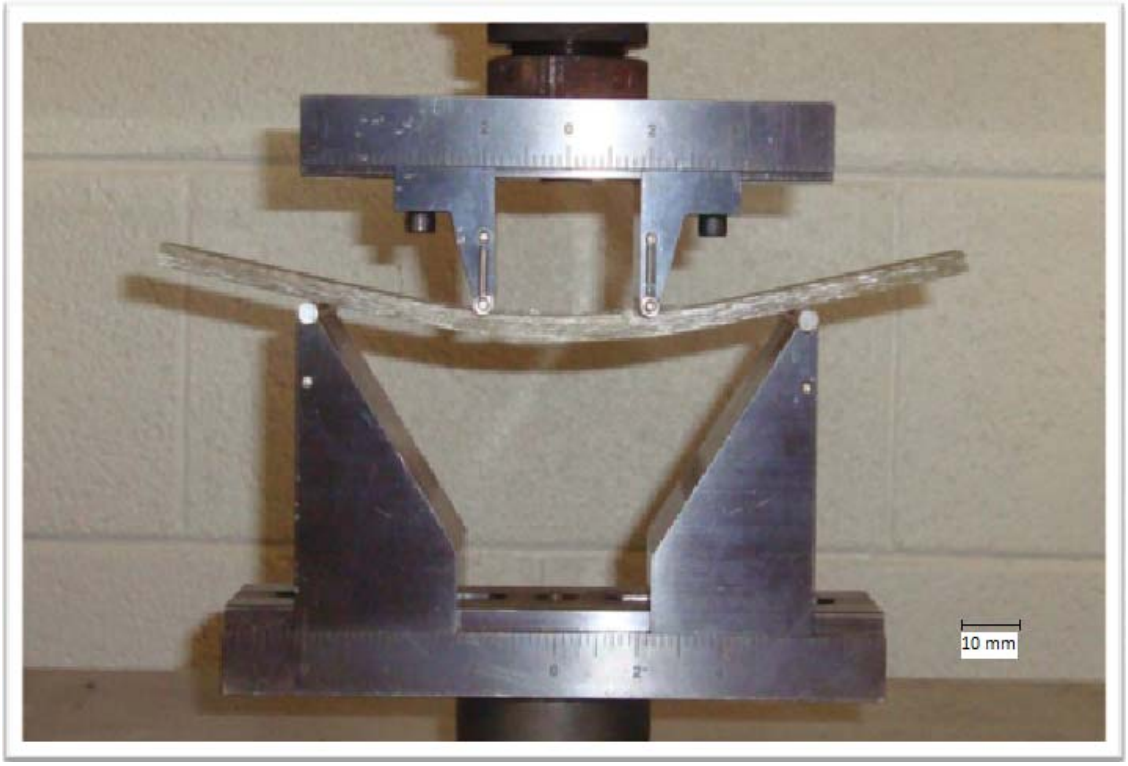

Fig.8 Four-point bending test

The distance between the loading noses (the load span) is one third of the support span (*67.7* mm). The length of support span was *203.2* mm which gave a *32:1* span-to-depth ratio. The specimen was deflected until failure occurred in the outer fibers.

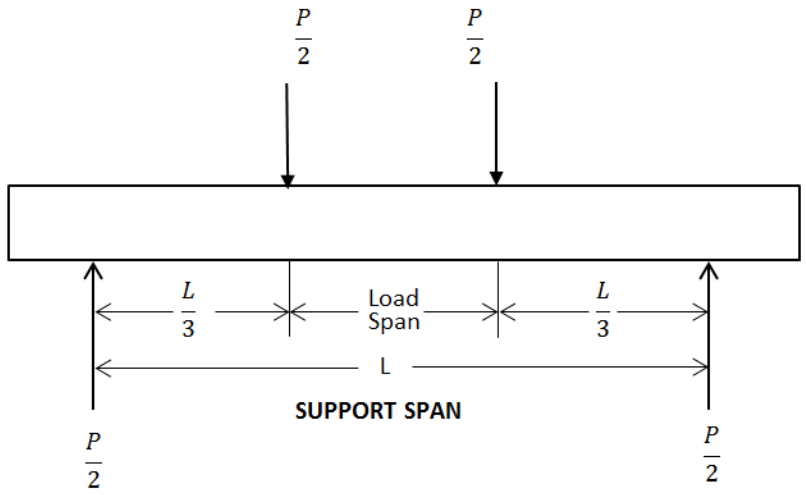

Fig.9 Schematic diagram of load application in four point bending test

Load and crosshead displacement were monitored and recorded. Maximum fiber stress was calculated considering large support spans and deflections in excess of 10% of the support span. The maximum stress at any point of load-deflection curve for a load span of one third of support span was determined by formula:

$$S = \left(\frac{PL}{bd^2}\right) \cdot \left[1 + \left(\frac{4.70D^2}{L^2}\right) - \left(\frac{7.04Dd}{L^2}\right)\right] \qquad (3.8)$$

where S is a stress in the outer fiber throughout the load span [*MPa*], P – load at a given point on the load deflection curve [*N*], L – support span [*mm*], b – width of beam [*mm*], d – depth of beam [*mm*], D – maximum deflection of the center of the beam [*mm*]

Maximum strain was calculated by using the formula:

$$r = \frac{4.70Dd}{L^2} \qquad (3.9)$$

where r – maximum strain in the outer fibers [*mm/mm*], D – maximum deflection of the center of the beam [*mm*], L – support span [*mm*], d – depth [*mm*].

3.6 Four-Point Bending Fatigue Tests

Fatigue testing was performed on a Bose Electroforce 3510 fatigue testing machine. The load cell has a 7.5 kN capacity. Figure 10 shows the 4-point bending fixture which was manufactured specially for this research. The fixture consists of upper and lower supports with rounded load points (radius *3.2* mm). Initially, end constraints were used to avoid longitudinal movement of a specimen during a test. But that method did not give desirable results because the end of the beam deflecting cyclically rubbed the constraint creating extra friction forces. Instead of end constraints, it was decided to make small grooves on each specimen at the point of contact with the support span. Post-failure inspection of the specimens proved that the groove was not a stress concentration point and did not have any influence on test results i.e. on location of the failure, its mode, etc. The seats of the fixture where specimen was placed on the supports were deepened with width of *25.6* mm which is slightly wider than a specimen and an undesired drift of a specimen in a transverse direction was prevented.

All the fatigue tests were performed with a support span length of *203.2* mm (*8* in), and load span was 1/3 of support span, just as with the static flexural tests. All fatigue tests were performed in load control condition at ambient temperature using sinusoidal loading. The load ratio was $R_{min}/R_{max} = 0.1$ for all the tests. The load values that correspond to desired stress levels were calculated in a similar way as it was done in static flexural tests.

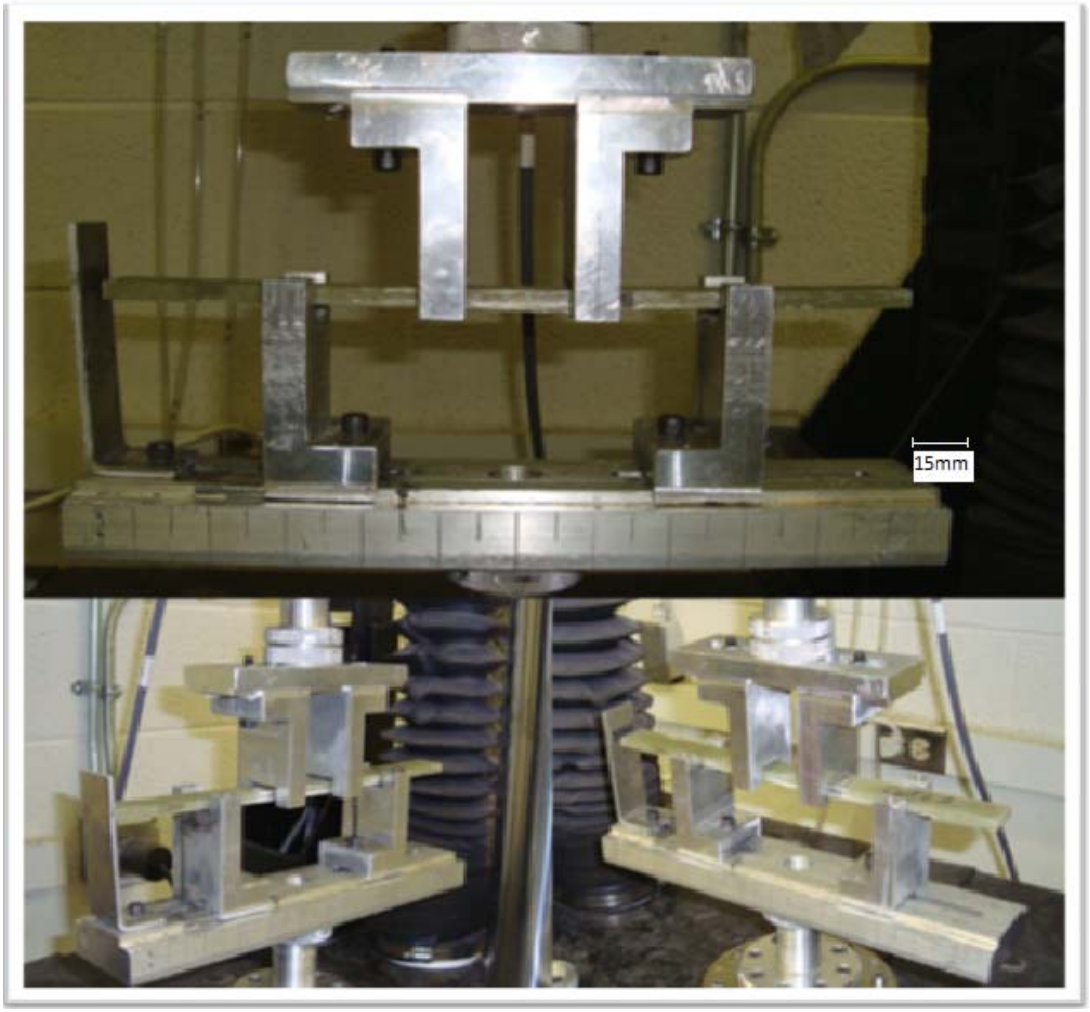

Fig.10 Four-point bending fixture for fatigue tests
(top) Front View
(bottom) Left and Right Views

CHAPTER IV

RESULTS AND DISCUSSION

4.1 Static Test Results

4.1.1 Uniaxial Test Results of Polyester Resin

Six test coupons were made from polyester resin. Concentration of hardener, curing time and other conditions were kept the same as for the composite material used in this study. Tests were conducted at ambient temperature.

Coupons were tested under uniaxial loading following the ASTM D3039 test method [36]. Dimensions of the coupons and test results are given in Table 6.

Table 6 Uniaxial test results of resin coupons

Coupon #	Length (mm)	Width (mm)	Thickness (mm)	Strength (MPa)	Strain	Elasticity Modulus (GPa)
RA-1	177.8	24.84	5.28	49.8	0.0176	2.95
RA-2	177.8	24.94	5.66	48.9	0.0178	2.80
RA-3	177.8	24.79	5.61	53.8	0.0200	2.81
RA-4	177.8	25.96	5.61	44.3	0.0155	2.60
RA-5	177.8	25.27	5.56	46.8	0.0163	2.90
RA-6	177.8	25.27	5.72	50.2	0.0182	2.90
Average	177.8	25.18	5.58	49.0	0.0180	2.827
STDV	0	0.40	0.14	3.2	0.0016	0.125

Figure 11 shows the broken resin coupons after testing. For all the specimens the location of the failure was away from grips. Some coupons failed on the top part, others in bottom part and mostly close to the middle section of a coupon. Failure type looked like combination of explosive and lateral failure somewhat similar to failure of brittle materials in which section is broken into shards.

Fig.11 Polyester resin coupons failed after uniaxial tensile test

Figure 12 shows stress strain curves of the tested samples. The average values for strength and modulus of elasticity for all samples are within 10%. The tensile strengths for coupons 1 and 3 are slightly less than for others but all are within acceptable limits.

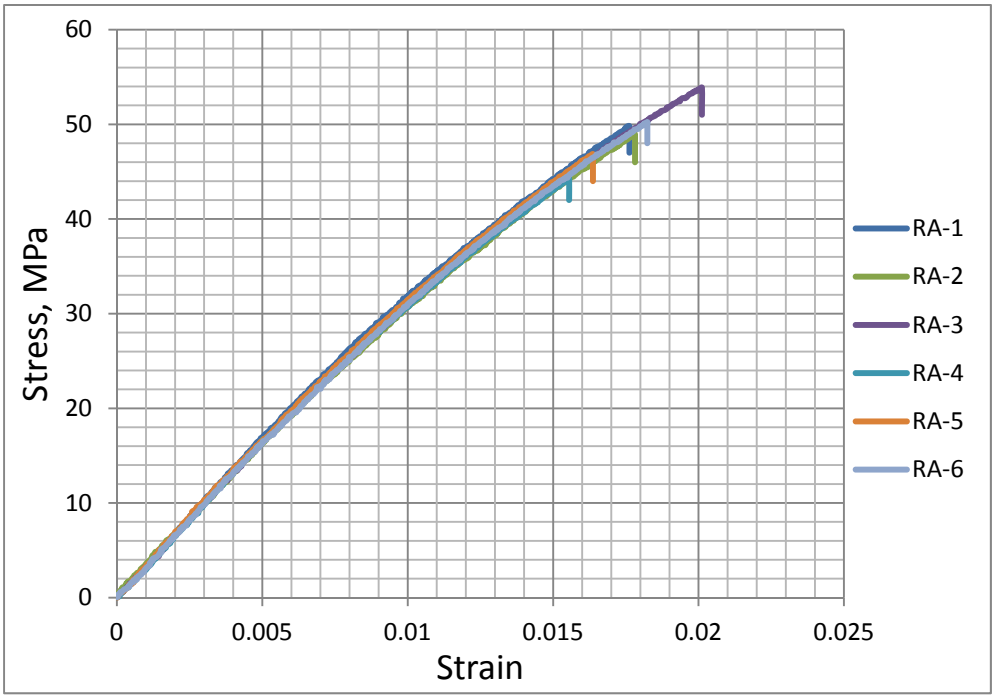

Fig.12 Stress-strain curves of polyester resin samples in uniaxial tension

4.1.2 Uniaxial Tests Results of the Composite Material

4.1.2.1 Longitudinal Direction

All coupons used for static uniaxial tests were composed of 2 layers. Tensile specimens were made thinner than bending specimens because of limitations of the testing machine. Thick coupons would require loads higher than the testing machine capacity. For example, the longitudinal uniaxial test load was about 18-20 kN for specimens tested in this study which was already almost a half of the testing machine capacity. Another problem was that high loads would require stronger bonding material for the steel tabs. The tab bond would likely fail before the actual failure of the material. The dimensions of longitudinal test coupons and results of static tests are shown in Table 7.

Table 7 Uniaxial test results of composite coupons in longitudinal direction

Coupon #	Length (mm)	Width (mm)	Thickness (mm)	Strength (MPa)	Strain	Elasticity Modulus (GPa)
Co 1	228.6	13.34	1.80	942.4	0.0255	36.9
Co 2	228.6	12.62	1.80	940.5	0.0240	39.2
Co 3	228.6	12.70	1.80	923.5	0.0252	36.7
Co 4	228.6	12.70	1.80	857.6	0.0225	38.2
Co 5	228.6	11.56	1.80	897.0	0.0232	38.6
Co 6	228.6	11.99	1.80	833.8	0.0215	38.7
Co 7	228.6	11.43	1.80	975.6	0.0258	37.8
Average	228.6	12.33	1.80	910.1	0.0240	38
STDEV	3E-14	7E-01	0E+00	50.3	0.0016	0.937

Figure 13 is a stress-strain plot of the tested samples. The standard deviations of strength and elastic modulus of tested coupons were about 5% of average values.

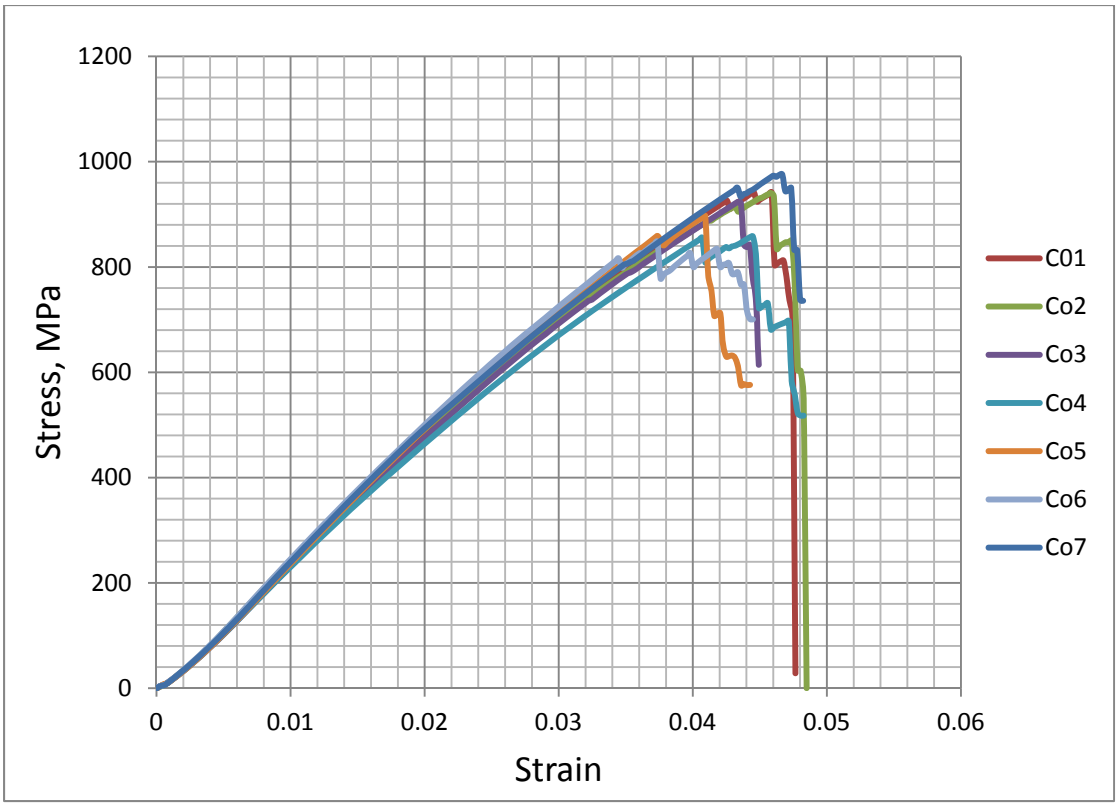

Fig.13 Stress-strain curves of longitudinal E-glass/Polyester composite coupons in uniaxial tension

The values of the strain on the plot are calculated using direct displacement measurement of testing machine, i.e. displacement of the load cell, while the strain and corresponding elastic modulus shown in Table 7 were measured using an electronic extensometer of 25 mm gage length. When the applied force was about 70-80% of failure force the device was taken off the coupon without interrupting the testing process. This was done because the arms of the extensometer are too sensitive to deflection and sudden failure of specimen might destroy it.

Figure 14 shows the specimens failed after uniaxial tensile loading. According to standard description provided in ASTM D3039 the failure of the specimens is classified as XGM-failure

where X-failure type, eXplosive

G-failure area, Gage

M-failure location, Middle

Fig.14 Characteristic failure pattern of E-glass/Polyester composite coupons after uniaxial tensile loading along the fiber direction

4.1.2.2 Transverse Direction

The results of static tests of transverse coupons under uniaxial loading are shown in

Table 8.

Table 8 Uniaxial test results of composite coupons in transverse direction

Coupon #	Length (mm)	Width (mm)	Thickness (mm)	Strength (MPa)	Strain	E Modulus (GPa)
CoT 1	152.4	25.76	1.80	52.4	0.0282	1.86
CoT 2	152.4	26.29	1.80	51.2	0.0272	1.88
CoT 3	152.4	25.20	1.80	43.2	0.0228	1.89
CoT 4	152.4	26.16	1.80	50.3	0.0276	1.82
CoT 5	152.4	25.40	1.80	51.4	0.0264	1.95
CoT 6	152.4	25.53	1.80	50.7	0.0271	1.87
Average	152.4	25.72	1.80	49.9	0.0266	1.88
STDEV	0	0.43	0	3.34	0.0019	0.041

Figure 15 is a plot of stress-strain curves of tested transverse samples. Strength of coupon #3 is markedly less than the strength of other coupons and looks like an obvious outlier. If we discard it as a simple chance error then the standard deviation of the strength reduces significantly to a value 0.8 MPa which is about 1.5% of the average strength.

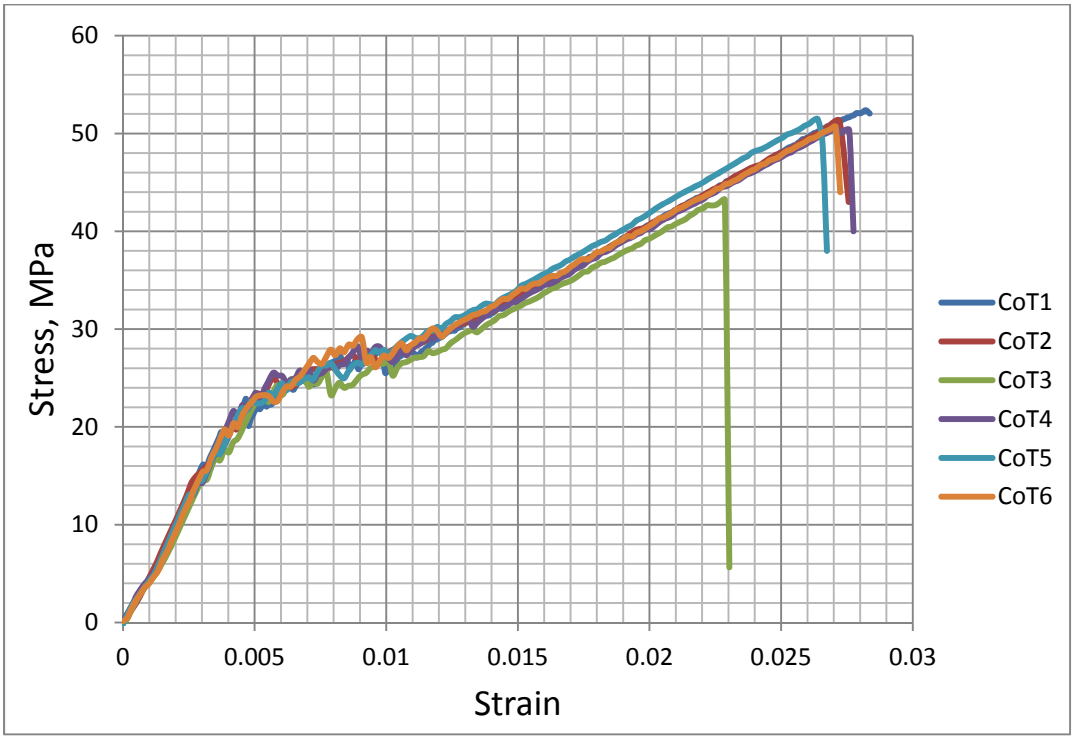

Fig.15 Stress-strain curves of transverse E-glass/Polyester composite coupons in uniaxial tension

At a strain of about 0.5% the stress-strain curve of transverse specimens showed a change of the slope. Initially the slope of the curve is high then through some sort of transition region it becomes much lower and remains constant up to failure. This slope change is due to the inhomogeneous structure of the fiber fabric. At first the applied load is carried by some fibers in the transverse direction and chopped fibers. This is the first and second section of stress-strain curve on the Figure 15. When the curve passes the transition region, the characteristic sounds of failing chops accompany the process. The

third part of the curve corresponds to a stage where the matrix of the composite carries the load. This conclusion comes from the fact that failure strain of the matrix is higher than that of fiber chops and that the third slope value is comparable to that of pure resin specimens. This behavior of the slope did not have a considerable influence on the research of the composite beam behavior. The stresses at which the beam was considered were much higher (by a factor of ~20) than this region.

Figure 16 shows transverse specimens failed under uniaxial loading. The lateral type of failure located close to the middle of a coupon was common for all the transverse specimens tested. According to ASTM 3039 standard description using three-part failure mode code, the failure of the specimens is classified as LGM-failure

where L-failure type, Lateral

G-failure area, Gage

M-failure location, middle

Fig.16 Characteristic failure pattern of E-glass/Polyester composite coupons after uniaxial tensile loading in transverse direction

4.1.3 Four-Point Bending Tests

4.1.3.1 Longitudinal Direction

Table 9 presents the results of the static bending tests on the composite beams carried following the ASTM D6272 test standard in the longitudinal direction of the fibers. All the specimens failed on the compressive surface of the beam by the same mode, i.e. compressive fiber microbuckling. The results of the tests were consistent, showing the standard deviation of less than 3% and 2% of average values of ultimate strength and elastic modulus, respectively.

Table 9 Four-point bending test results of composite beams in longitudinal direction

Coupon #	Support Span (mm)	Width (mm)	Thickness (mm)	Strength (MPa)	Strain	Flexural Modulus (GPa)
CoBL 1	203.2	25.91	6.38	919.6	0.0220	46.7
CoBL 3	203.2	24.84	6.40	942.0	0.0225	47.6
CoBL 4	203.2	24.51	6.35	997.3	0.0236	47.9
CoBL 5	203.2	25.12	6.32	939.3	0.0219	48.9
CoBL 6	203.2	26.19	6.35	956.3	0.0219	48.8
CoBL 7	203.2	25.02	6.35	958.1	0.0228	48.7
Average	203.2	25.26	6.36	952.1	0.0225	48.1
STDV	3E-14	0.65	0.03	26.15	0.0007	0.865

Figure 17 is the plot of stress-strain curve of the composite beam tested under static 4-point bending loading. The values of stress and strain were determined using the procedure described in ASTM D6272 [38]. The consistency of the test results can be seen on this plot.

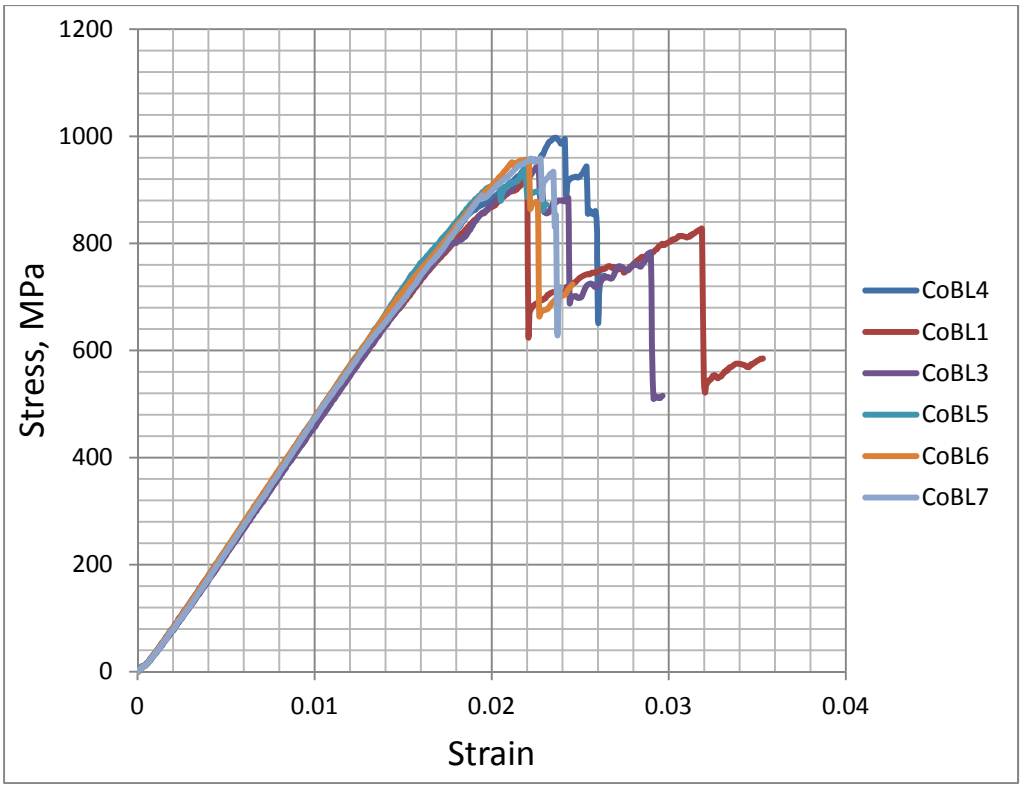

Fig.17 Stress-strain curves of E-glass/Polyester composite beams in four-point bending in longitudinal direction

The Figure 18 is a picture of a longitudinal bending specimen showing typical compression failure.

Fig.18 Typical failure of E-glass/Polyester composite beams in four-point bending in longitudinal direction

4.1.3.2 Transverse Direction

Table 10 lists the test results of four-point bending tests of the composite beam samples, tested under static loading in transverse direction of the fibers. The low standard deviation of the test results shows the good consistency between test results of different samples.

Table 10 Four-point bending test results of composite beams in transverse direction

Coupon#	Support Span (mm)	Width (mm)	Thickness (mm)	Strength (MPa)	Strain	Flexural Modulus (GPa)
CoBT11	203.2	26.04	6.48	125.0	0.0196	6.38
CoBT12	203.2	25.60	6.48	121.5	0.0184	6.60
CoBT13	203.2	24.89	6.48	128.0	0.0209	6.12
CoBT14	203.2	25.53	6.43	130.2	0.0195	6.68
CoBT15	203.2	25.40	6.45	131.6	0.0191	6.89
CoBT16	203.2	25.65	6.50	125.3	0.0182	6.88
Average	203.2	25.52	6.47	126.9	0.0193	6.59
STDV	3E-14	0.37	0.03	3.73	0.001	0.299

Figure 19 is the stress strain-curve of composite beams tested in the transverse direction. This curve is comparable to the curve that was obtained from uniaxial tests in transverse direction of the fibers. The change in slope is analogous to that observed in uniaxial tests and described in section 4.2.2.

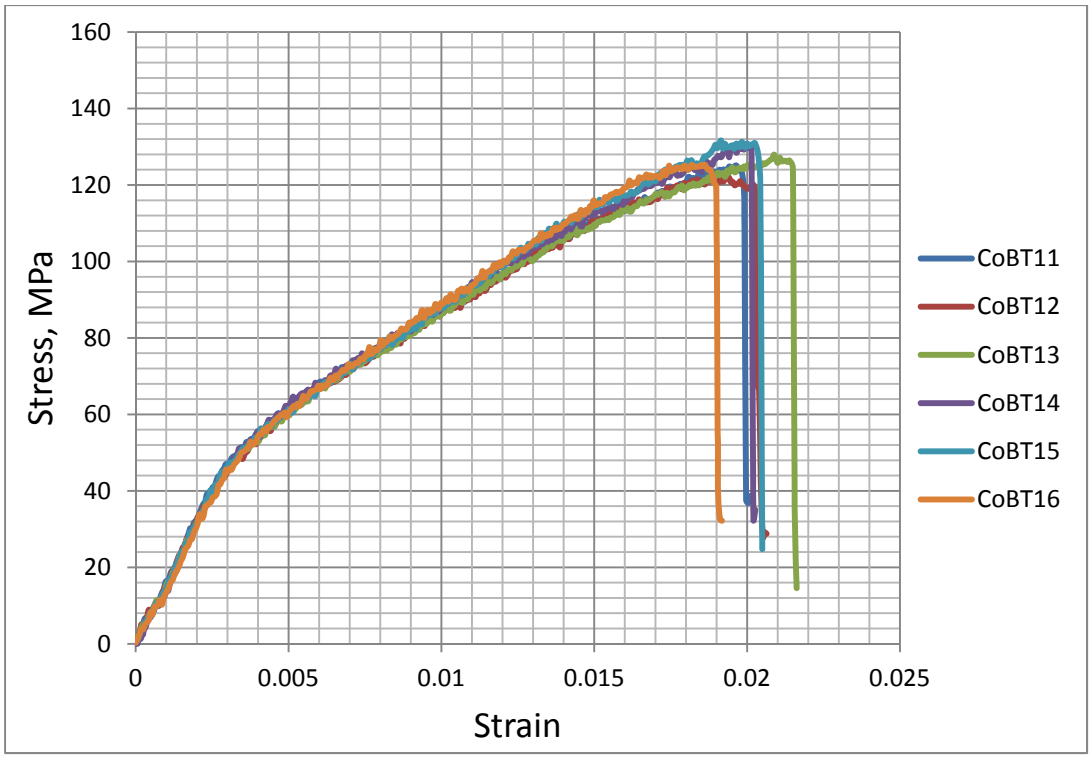

Fig.19 Stress-strain curves of E-glass/Polyester composite beams in four-point bending in transverse direction

4.2 Finite Element Analysis: ANSYS Results

Finite element (FE) stress analysis was performed in order to understand the distribution of stresses in a multilayered composite beam. Also, possible stress concentrations around points of contact and load application needed to be evaluated. Modeling of specimen for stress analysis was done with ANSYS software package, version 13.0. The element used in modeling was solid185. Solid185 is used for 3-D modeling of solid structures. It is defined by eight nodes having three degrees of freedom at each node: translations in the nodal x, y, and z directions. The element has plasticity, hyperelasticity, stress stiffening, creep, large deflection, and large strain capabilities. It also has mixed formulation capability for simulating deformations of nearly incompressible elastoplastic materials and fully incompressible hyperelastic materials [39].

The material properties needed for modeling were determined from experimental test results or found using basic principles of mechanics of composite materials and considering properties of constituent materials of the composite.

E_{11} and E_{22}, E_{33} come from experimental results.

$G_{12}$and G_{13} were determined using Halpin-Tsai semiempirical relation of the form:

$$G_{12} = G_m \frac{(1 + v_f)G_{12f} + v_f G_m}{v_m G_{12f} + (1 + v_f)G_m} \qquad (4.1)$$

If $G_m = 1.074\ GPa, G_{12f} = 28.3\ GPa$, $v_f = 0.50$ then $G_{12} = 2.93\ GPa$

For a unidirectional material, the 2-3 plane is practically isotropic, so $E_2 = E_3$ and $G_{12} = G_{13}$

For a transversely isotropic material (with 2-3 plane of isotropy) the transverse shear modulus is related to the transverse Young's modulus and Poisson's ratio by the familiar isotropic relation:

$$G_{23} = \frac{E_2}{2 \cdot (1 + \nu_{23})} \qquad (4.2)$$

If $E_2 = 1.470\ GPa$, $\nu_{23} = 0.23$, then $G_{23} = 0.57\ GPa$.

The material properties that were used in FE analysis are summarized in a following Table 11.

Table 11 Summary of mechanical properties of composite beam for ANSYS model

Longitudinal Elastic Modulus, E_{11} (GPa)	36.2
Transverse Elastic Modulus, E_{22} (GPa)	1.47
Elastic Modulus through the thickness, E_{33} (GPa)	1.47
Shear Modulus, 1-2 plane, G_{12} (GPa)	2.93
Shear Modulus, 1-3 plane, G_{13} (GPa)	2.93
Shear Modulus, 2-3 plane, G_{23} (Gpa)	0.49
Poisson's ratio, 1-2 plane, v_{12}	0.29
Poisson's ratio, 1-3 plane, v_{13}	0.50
Poisson's ratio, 2-3 plane, v_{23}	0.29
Tensile Strength, F_1 (MPa)	920
Tensile Strength, F_2 (MPa)	51

The actual overall specimen dimensions were used in FE model and the ANSYS results were compared to experimental results. The dimensions of the FE specimen are shown in Table 12.

Table 12 Specimen geometry for ANSYS model

	inch	meter
Length	8	0.203
Width	0.965	0.0245
Thickness	0.25	0.00635

FE boundary conditions used are as follows:

1) Two ends of specimen were constrained along edge lines in Z direction.
2) One node from each side was constrained in Y direction
3) One center node of the beam was constrained in X direction which prevented lateral movement of the beam as the load was applied.
4) Total load was divided into 20 point loads and was applied on 10 nodes along 2lines dividing load span into 3 equal parts ($L/3 = 0.203/3$) as described in ASTM D6272.

   The end loads were divided into half a load because in such a way it is more close to line load.
5) The number of elements through the thickness of the beam was equal to 8, to represented 8 layers of the beam tested.

Figues 20 and 21 show the front and isometric views, respectively, of the FE beam with constraints and loads applied.

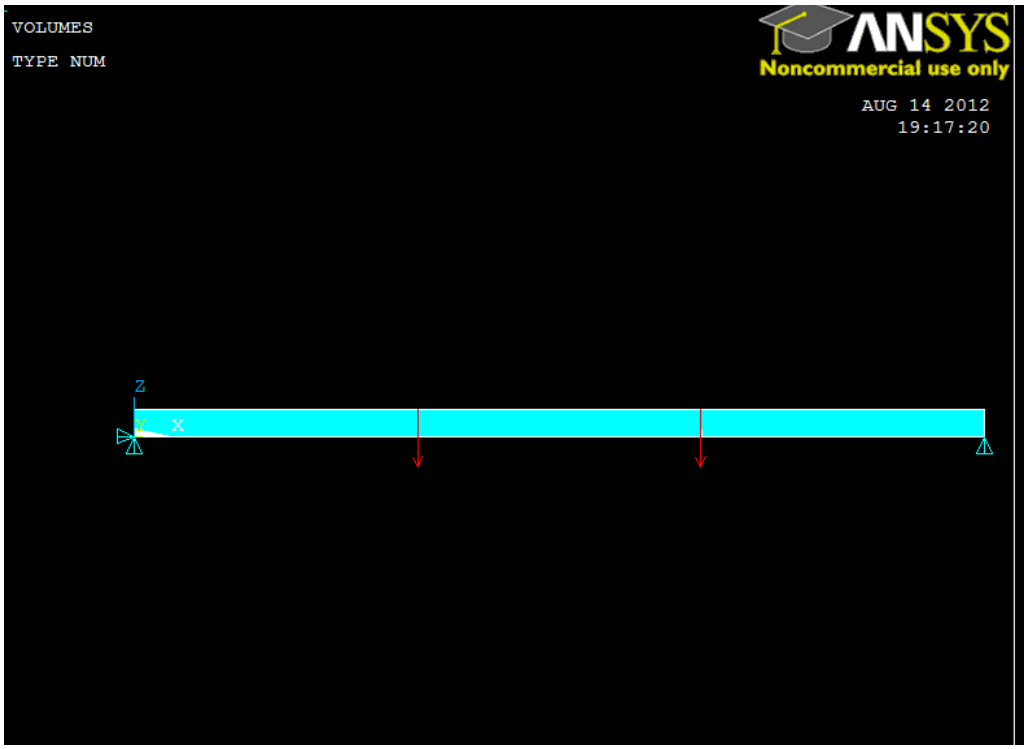

Fig.20 Schematic diagram of the loading and constraints of composite beam in ANSYS (Front View)

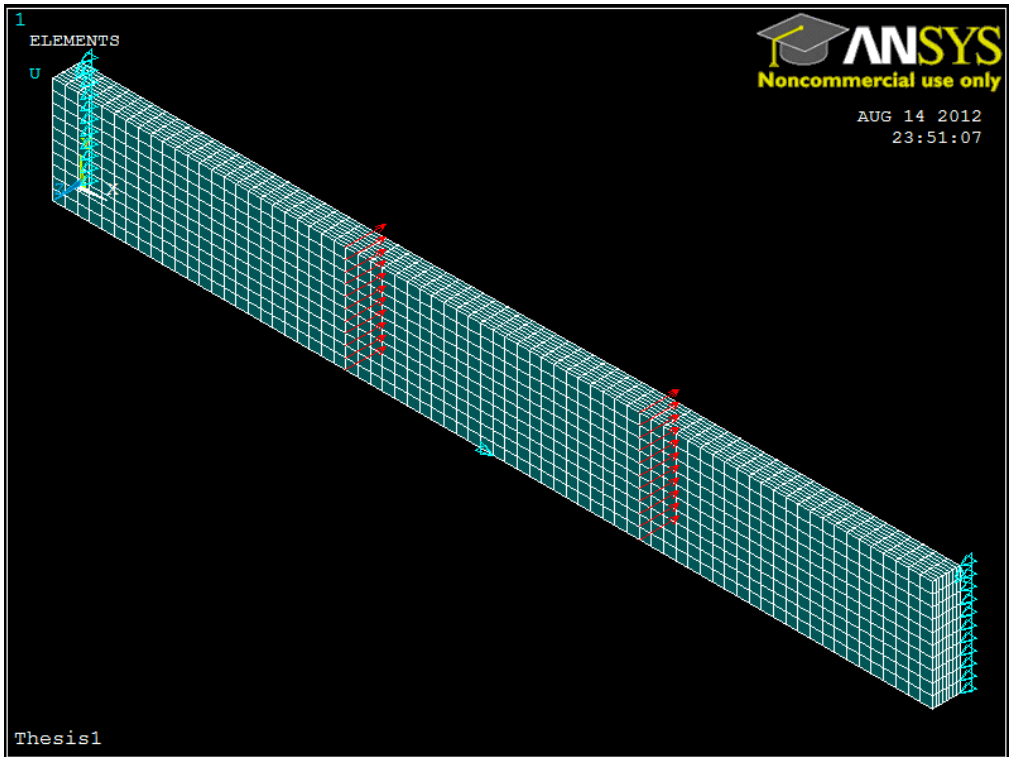

Fig.21 Schematic diagram of the loading and constraints of composite beam in ANSYS (Isometric View)

The real specimen's experimental results were used in the analysis to make a comparison between ANSYS model and test results. A load of 3745 N was applied to the beam which was about 85% of the static failure load of this beam. Table 13 shows the summary of results obtained from ANSYS model.

Table 13 Summary of ANSYS solution of the composite beam

	Experimental Results	ANSYS Results
Applied Force (N)	3745	3745.0
Deflection (mm)	24.1	27.0
Equivalent Stress (MPa)	-	785.0
Max. Stress X-direction (MPa)	800.8	789.0
Max. Stress Y-direction (MPa)	-	8.7
Max. Stress Z-direction (MPa)	-	42.1
Max. Shear Stress XZ plane (MPa)	-	22.5

Figure 22 shows a contour plot of the nodal solution of the X-component of the stress which corresponds to stress along the direction of the fibers.

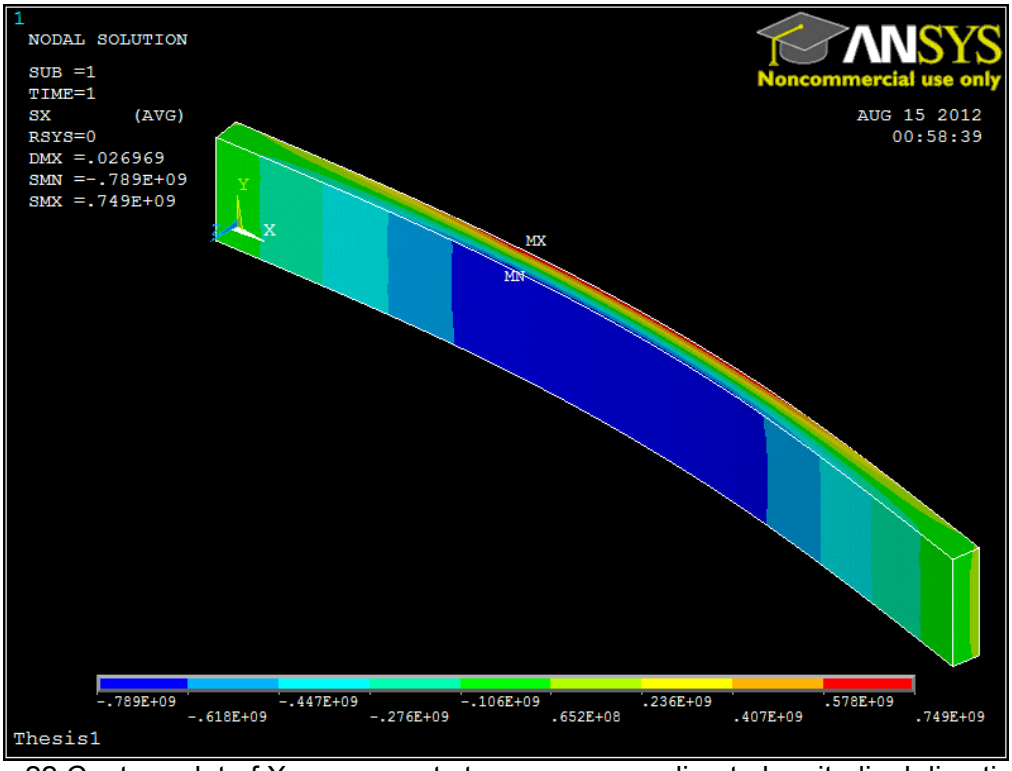

Fig.22 Contour plot of X-component stress corresponding to longitudinal direction

From Fig.22, it is clearly seen that highest compressive (blue) and tensile stresses (red) are on outer layers of the beam and they equal 789 MPa and 749 MPa, respectively. The maximum displacement of the beam is equal to 26.9 mm.

Following ASTM D6272, the maximum experimental stress, for an applied load of 3745 N was 800 MPa. This value differs from the stresse predicted by ANSYS by less than 4%. Experimental displacement was 24 mm, 10% different than the ANSYS results.

The area of high stress shown in Fig.22 is at a similar location as the damaged area in the real specimen (Fig. 23). All the coupons during static test failed by the same way, i.e. failure was on the compressive side of compression and the damaged area was almost the same. Apparently, the composite material that was studied is stronger in tension rather than in compression when a static load is applied.

Fig.23 Failure of E-glass/Polyester composite beams in four-point bending in longitudinal direction

Figure 24 shows the locations of highest Von Mises Equivalent stress. In the case of composites, the regions of highest stress are not necessarily the locations of failure. But the figure illustrates the distribution of stresses through the beam.

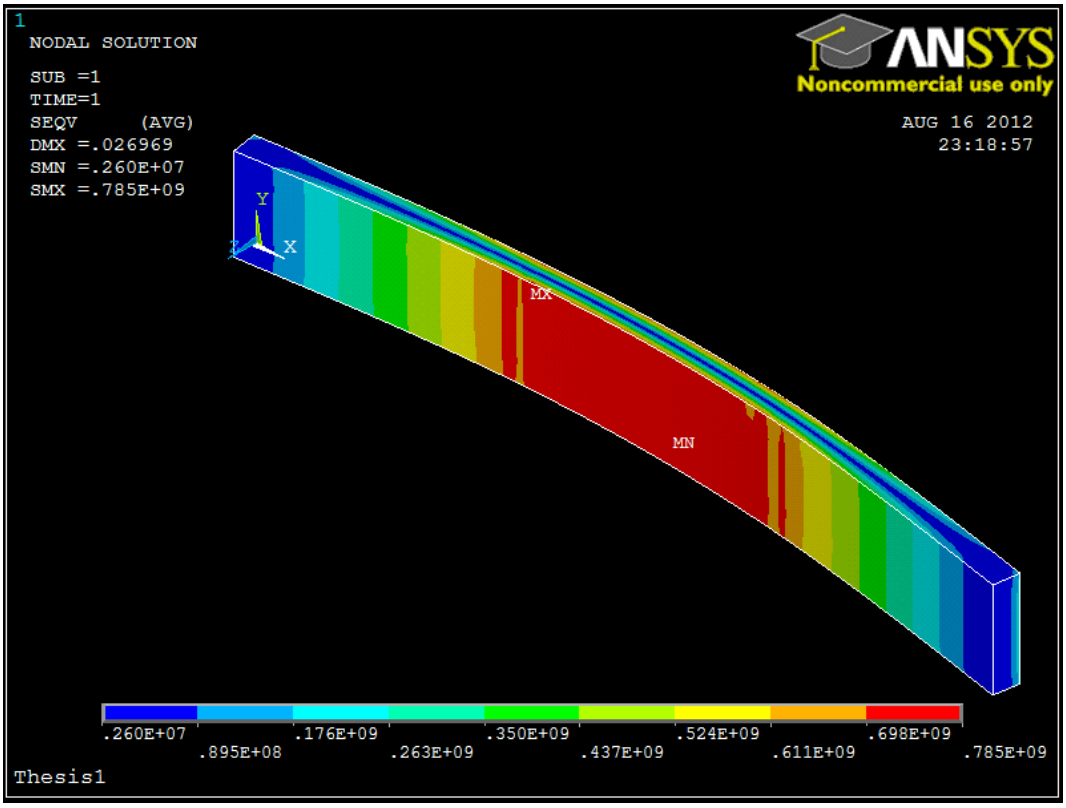

Fig.24 Contour plot of equivalent stress

Figures 25 and 26 show the stresses in the Y and Z directions, respectively. There are obvious locations of stress concentrations which correspond to points of load applications. The highest value in the Y direction (Fig 25) was 8.7 MPa of compression, and in the Z direction (Fig 26) it was about 42 MPa of compressive stress. Visual inspection of the experimental coupons revealed no damage at the points of load application.

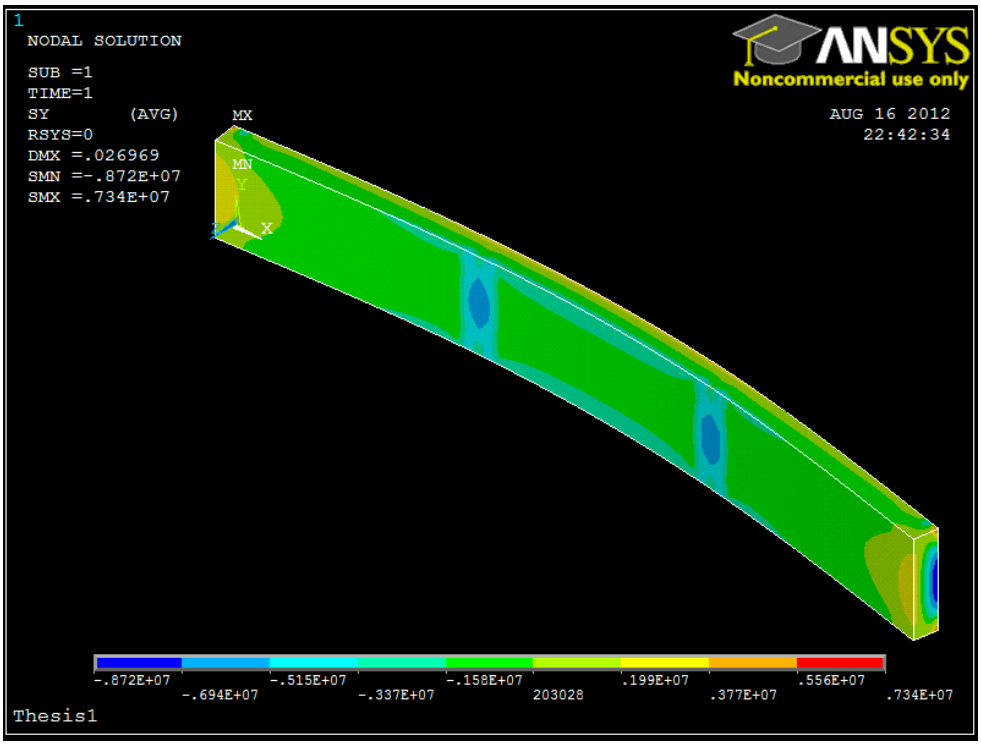

Fig.25 Contour plot of Y-component stress corresponding to transverse direction

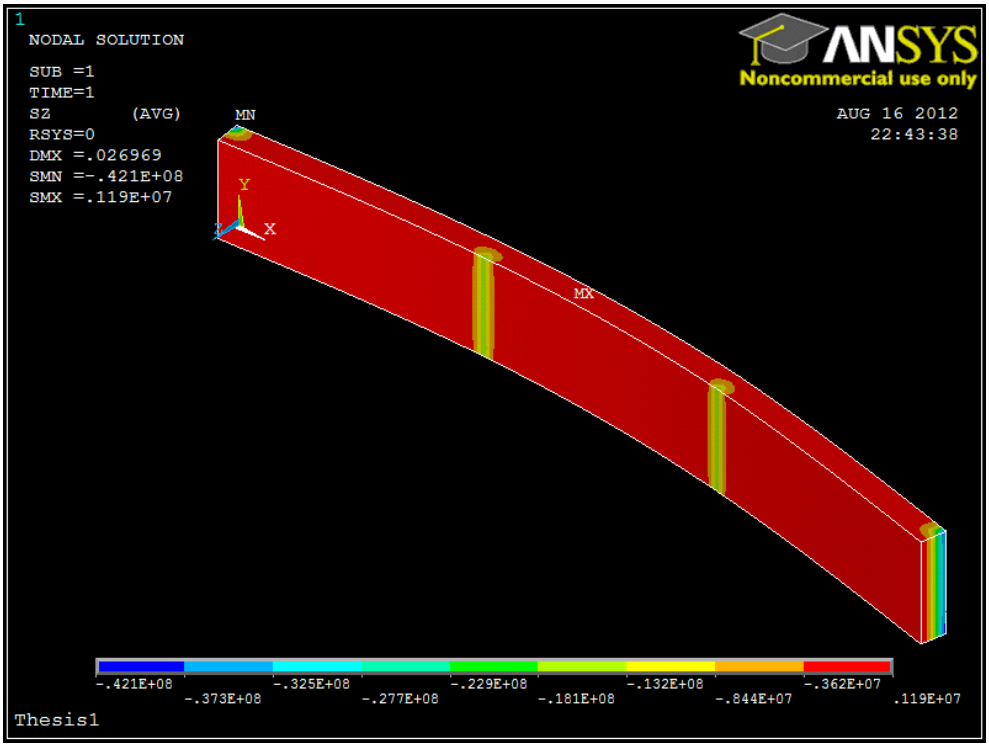

Fig.26 Contour plot of Z-component stress corresponding to direction through the thickness of the beam

As expected, the highest shear stresses were observed at the midplane of the beam. The highest value of the stress reached 22.5 MPa. It was previously mentioned that we had two orientations of lying of plies: clean face to clean face and chopped face to chopped face. In the case of chops facing each other, we had shear failure in the midplane just like it is shown in Figure 27. Failure originated on either side of the beam and continued along about 1/3 of the total length. In the case of clean sides of the plies facing each other, no shear failure was observed. This was the orientation used for tensile and fatigue tests.

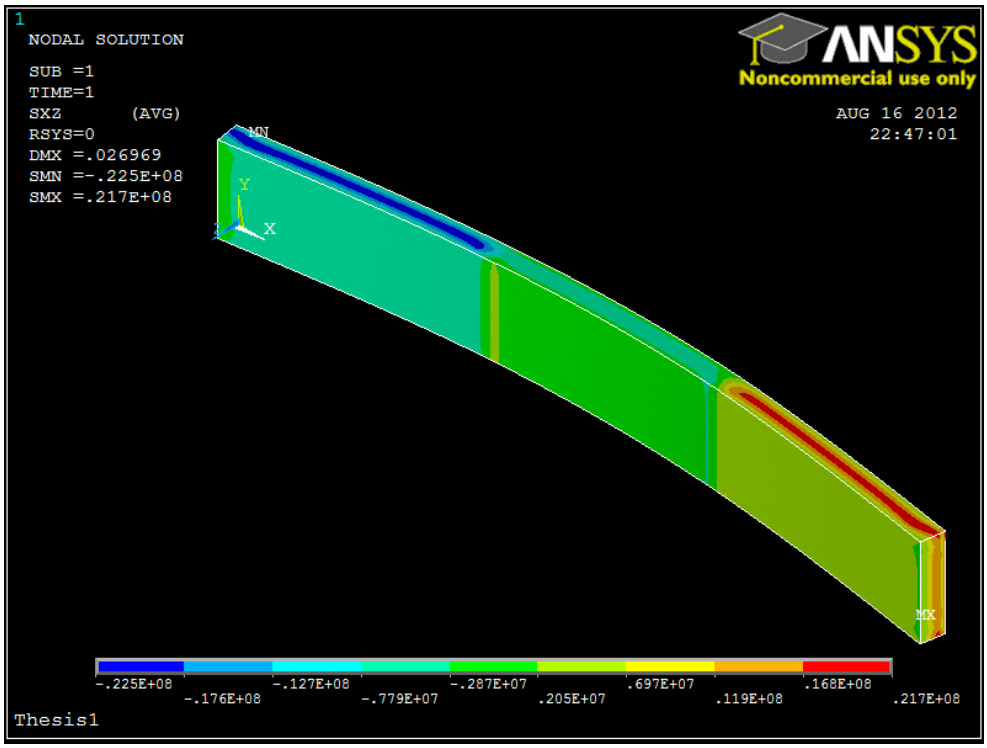

Fig.27 Contour plot of XZ-component stress corresponding to interlaminar shear stress of the beam

4.3 Stress versus Number of Cycles: Fatigue Test Results

The results of fatigue experiments are plotted in Figure 28. The S represents the maximum applied stress and N is the corresponding fatigue life. The load ratio, S_{min}/S_{max}, in this research was equal to $R = 0.1$.

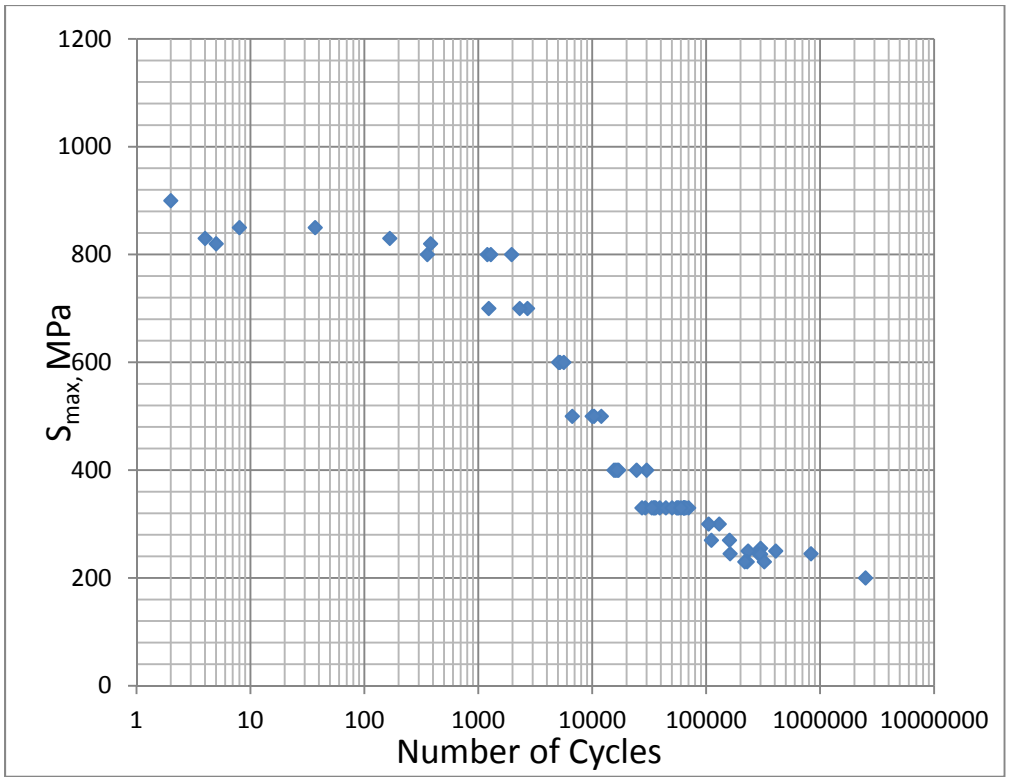

Fig.28 S-N curve of E-glass/Polyester composite beam tested in four-point bending fatigue load in longitudinal direction

The summary of specimen dimentions and fatigue test results at R=0.1are presented inTable 14.

Table 14 Fatigue test results (R=0.1)

Specimen Number	Width (mm)	Depth (mm)	Support Span (mm)	Applied Stress (MPa)	Number of cycles to failure	Test Frequency (Hz)
CoFL 6	24.51	6.38	203.2	245	830620	8
CoFL 7	24.54	6.40	203.2	200	2055838	8
CoFL 8	24.26	6.38	203.2	300	128575	8
CoFL 1	24.69	6.35	203.2	270	157753	8
CoFL 2	23.32	6.40	203.2	255	297845	8
CoFL 3	24.46	6.38	203.2	330	70737	8
CoFL 4	23.24	6.40	203.2	500	12000	6
CoFL 13	23.37	6.53	203.2	400	15000	4
CoFL 23	24.00	6.38	203.2	600	5200	4
CoFL 17	23.88	6.35	203.2	700	2700	3
CoFL 19	24.13	6.22	203.2	800	1959	3
CoFL 15	24.13	6.30	203.2	800	1200	3
CoFL 22	24.28	6.40	203.2	700	2307	4
CoFL 9	24.64	6.35	203.2	330	64250	8
CoFL 10	25.15	6.35	203.2	250	407550	8
CoFL 12	24.26	6.35	203.2	300	106930	8

Table 14 (Cont.)

CoFL 20	25.02	6.35	203.2	245	287898	8
CoFL 21	24.89	6.30	203.2	245	300000	8
CoFL 24	24.38	6.32	203.2	400	24480	6
CoFL 14	24.38	6.32	203.2	500	9980	3
CoFL 11	24.46	6.35	203.2	800	1286	1
CoFL 16	25.07	6.32	203.2	850	8	1
CoFL 18	24.51	6.38	203.2	900	2	1
CoFL 25	24.84	6.32	203.2	820	5	1
CoFL 5	24.51	6.35	203.2	830	4	1
CoFL26	24.69	6.32	203.2	250	233538	8
CoFL37	25.40	6.27	203.2	330	29187	8
CoFL38	24.92	6.25	203.2	270	111000	8
CoFL29	25.07	6.30	203.2	245	162000	8
CoFL36	25.02	6.35	203.2	400	15500	6
CoFL32	24.87	6.30	203.2	230	228812	8
CoFL39	24.84	6.30	203.2	500	6672	8
CoFL30	24.77	6.30	203.2	330	39093	8
CoFL28	24.69	6.30	203.2	230	216000	8
CoFL33	24.66	6.30	203.2	400	16926	6
CoFL43	24.64	6.32	203.2	400	16632	10
CoFL27	24.59	6.32	203.2	330	34491	10
CoFL40	24.00	6.30	203.2	330	35006	10
CoFL41	24.13	6.20	203.2	330	32994	10
CoFL42	24.46	6.27	203.2	330	35579	6
CoFL31	23.88	6.22	203.2	330	27306	6
CoFL34	24.08	6.30	203.2	330	33294	8
CoFL35	24.49	6.30	203.2	330	44250	8
CoFL50	24.28	6.48	203.2	330	54944	10
CoFL51	24.89	6.38	203.2	330	57432	10
CoFL52	24.38	6.48	203.2	330	56134	10
CoFL57	24.03	6.40	203.2	330	63498	6
CoFL58	24.26	6.45	203.2	330	50168	6
CoFL59	24.97	6.45	203.2	330	63000	6
CoFL47	25.27	6.48	203.2	330	63995	8
CoFL44	25.15	6.43	203.2	330	66097	8
CoFL46	25.02	6.48	203.2	330	60000	8
CoFL55	25.30	6.43	203.2	230	323260	12
CoFL61	25.27	6.48	203.2	500	10364	5
CoFL54	24.89	6.43	203.2	600	5067	3
CoFL48	24.89	6.43	203.2	600	5624	3
CoFL49	24.79	6.48	203.2	700	1235	3
CoFL56	24.74	6.48	203.2	800	357	3
CoFL53	24.69	6.45	203.2	820	381	2
CoFL45	24.49	6.48	203.2	830	167	2
CoFL60	24.46	6.48	203.2	850	37	2

In Figure 29 both compression and tension sides of 9 different specimens are shown in the order of applied stress level from 230 MPa to 900 MPa. For low stress levels from

230 MPa to 500 MPa failure on the tension side of specimens dominates. The compression side of the specimens has no failure; as the stress increases, some transverse lines start appearing indicating initiation of failure. Further, when the stress level increases from 600 to 900 MPa, the damage area on the compression side gets wider while the tension side damage decreases. At high stresses, over 850 MPa, all specimens failed on the compression side of the beam. On the S-N graph, the change of failure mode from tension to compression corresponds to transition region where sudden decrease in the life is observed.

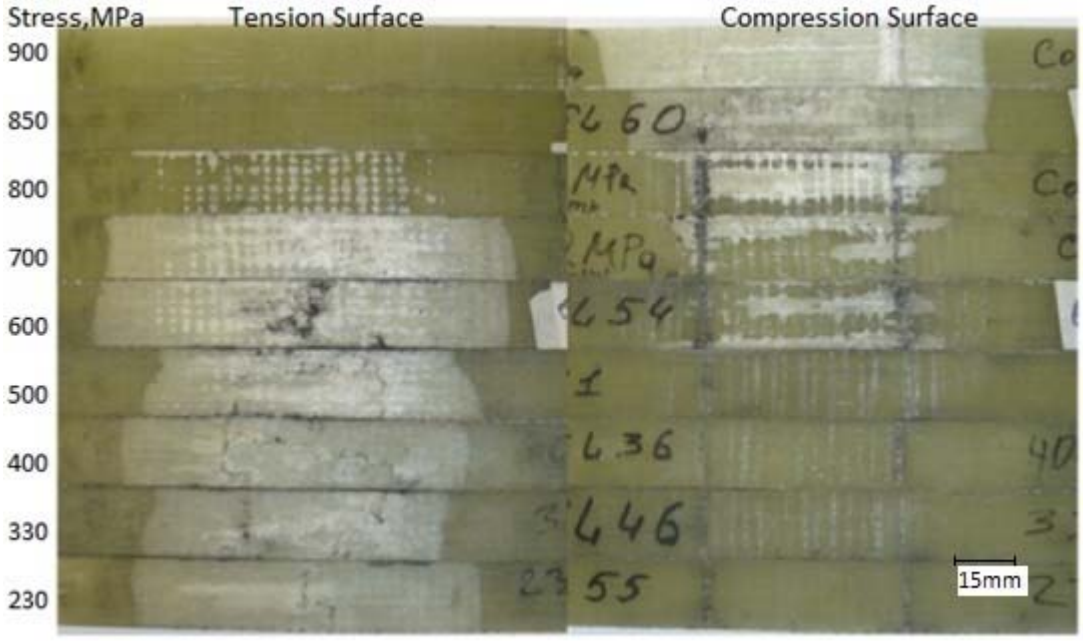

Fig.29 Progressive failure pattern of E-glass/Polyester composite beams in four-point bending fatigue load in longitudinal direction

4.4 Model Calculation

4.4.1 Low Cycle fatigue Region, Compressive Failure

According to researchers [26] in polymer matrix composites the kink band fiber rotation angle, $\overline{\varphi}$, with its initial fiber misalignment, $\overline{\varphi}$, is in the range of $3° - 5°$ or $0.052 - 0.087$ radians. The angle between kink band and direction, normal to the fibers

(Fig.1)$\beta = 20°$ is typical for many unidirectional fiber composites [40]. Compressive strength obtained from results of four-point bending experiments is $\sigma_c^{\infty} = 920\ MPa$. The transverse tensile strength is $\sigma_{Ty} = 50\ MPa$. We can determine approximate shear strength for the given material using expression of Budiansky and Fleck. Solving Eq.2.28 for the shear yield stress shows that $\tau_y = 30 - 62\ MPa$ (for the range of angle $3° - 5°$) or the average value is $\tau_y = 46\ MPa$.

For the Slaughter-Fleck model the non-dimensional variables of equations *2.29* and *2.30* have to be determined. The parameter *R* from Eq.2.33 defining the eccentricity of the yield ellipse is equal to $R = 50/46 = 1.08$. Assuming that $\beta = 20°$, from Eq.2.32 the parameter α equal to $\alpha = \sqrt{1 + 1.08^2 tan^2 20} = 1.19$

The shear modulus of the composite, obtained previously for ANSYS model is $G = 2.93\ GPa$

From the shear yield stress the shear yield strain can be found as:

$$\gamma_y = \frac{\tau_y}{G} = \frac{46}{2930} = 0.0158 \qquad (4.3)$$

The adjusted shear modulus and shear strain from Eq.2.30 are $G^* = 1.19^2 \times 2.93 = 4.15\ GPa$ and $\gamma_y^* = 0.0158/1.19 = 0.0133$

The non-dimensional variables from Eq.2.29 are $S_c^{\infty} = 920/4140 = 0.22$ (critical strength related value) and $\bar{\omega} = 0.0698/0.0133 = 5.25$ (kink band angle related value).

Substituting values for critical strength and kink band angle into Eq.2.31, it can be solved for the Ramberg-Osgood parameter *n*:

$$0.22 = \frac{1}{1 + n\left(\frac{3}{7}\right)^{1/n}\left(\frac{5.25}{n-1}\right)^{(n-1)/n}} \qquad (2.31)$$

Solving Eq.2.31 we get $n = 2.33$.

Table 15 is the summary of the parameters determined for the model.

Table 15 Summary of parameters for Slaughter's model

Para-meter	σ_c^{∞}	σ_{Ty}	τ_y	G	G^*	γ_y	γ_y^*	S_c^{∞}	$\overline{\omega}$	R	α	n
Value	920 MPa	50 MPa	46 MPa	2.93 GPa	4.15 GPa	0.0158	0.0133	0.22	5.25	1.08	1.19	2.33

With a Ramberg-Osgood parameter, $n = 2.33$, we can solve Eq.2.33 for t_2 for any S_{max} and then solve eq.2.34 for Δt. Using Eq.2.32, we can then determine the effective plastic strain, $\Delta\eta$.

Finally, a Coffin-Manson type relationship, eq.2.35, is used to determine the fatigue life, N_f.

$$\frac{\Delta\eta}{2} = \frac{\gamma_f'}{y_y}(2N_f)^c \qquad (2.38)$$

The material parameters γ_f' and c were varied within ranges suggested by researchers [25] to determine the best values that fit the fatigue test data of the material. The upper limit of applied stress was determined from Eq.2.40:

$$S^{\infty} = (1 - 0.1)920 \approx 830\ MPa \qquad (2.40)$$

The results of calculation of fatigue life of the composite beam for varied applied stress levels are presented in Table 16.

Table 16 Results of calculation of fatigue life using Slaughter's model

Max. Stress (MPa)	S_{max}^{∞}	S_{min}^{∞}	t_2	Δt	$\Delta\eta$	Number of Cycles to Failure			
						Model 1 $c = -0.55$ $\frac{\gamma_f'}{y_y} = 10$	Model 2 $c = -0.5$ $\frac{\gamma_f'}{y_y} = 20$	Model 3 $c = -0.7$ $\frac{\gamma_f'}{y_y} = 40$	Model 4 $c = -0.8$ $\frac{\gamma_f'}{y_y} = 40$
830	0.20	0.020	-	-	-	1	1	1	1
830	0.20	0.020	1.66	1.33	0.379	677	2387	1046	402
800	0.19	0.019	1.48	1.19	0.303	1016	3586	1440	532
600	0.14	0.014	0.91	0.73	0.114	6014	21209	5820	1806
500	0.12	0.012	0.75	0.6	0.077	12275	43288	10195	2949
400	0.10	0.010	0.60	0.48	0.049	27921	98461	19446	5189
200	0.05	0.005	0.28	0.22	0.010	502160	1770800	188284	37830
180	0.04	0.004	0.22	0.18	0.007	960467	3386959	313402	59082

Figure 30 shows a comparison between the experimental fatigue data and the Slaughter's model predictions with different parameters.

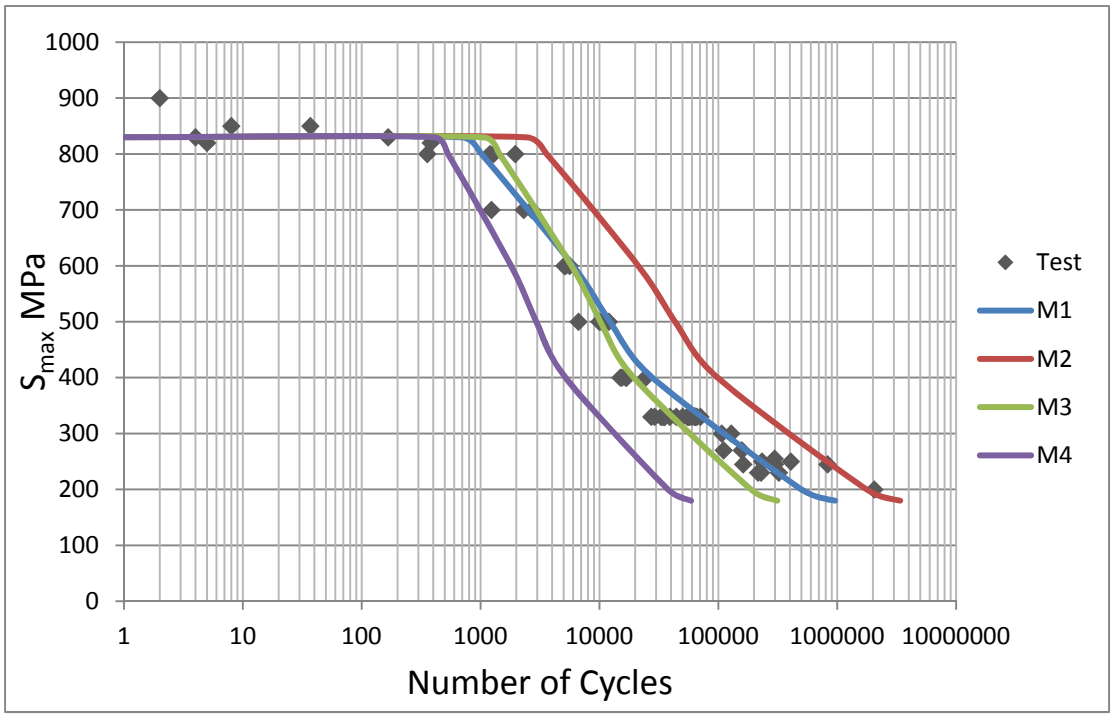

Fig.30 Slaughter's model predictions with four different parameters compared to experimental data

Model 3 ($c = -0.7;\ y_f' = 40$) looks to be in the best agreement with the test data. Here only the low cycle fatigue region (less than 30000 cycles) was considered. This is because model was developed for compressive fatigue and only applies to the region of S-N curve where compressive failure occurs.

4.4.2 High Cycle Fatigue Region, Tensile Failure

The high cycle fatigue (HCF) region of most composite materials is well-predicted by a power law equation. The form of the equation is:

$$S = AN_f^n \tag{4.4}$$

Experimental data can be used in order to obtain parameters A and n. Equation 4.4 can be rewritten in the form:

$$\log S = \alpha \log N_f + \beta \tag{4.5}$$

where β is the intercept at $N_f = 1$, and α is the slope of the curve. N_f is the fatigue life.

Parameters α and β are the material constants and related to the *A* and *n* by:

$$A = 10^{\beta} \tag{4.6}$$

$$n = \alpha \tag{4.7}$$

Taking $\log S$ *as Y* and $\log N_f$ *as X* a linear regression analysis on the test results is used to determine these constants. Table 17 lists the test data that was used for the regression analysis.

Table 17 Fatigue test results of composite beam in HCF region used for regression analysis

Max.Stress *S* (MPa)	Number of cycles N_f	Log(S) Y	Log(N_f) X
200	2055838	2.301	6.313
230	256000	2.362	5.408
245	395000	2.390	5.597
250	320000	2.398	5.505
270	134000	2.431	5.127
300	128000	2.477	5.107
330	45000	2.519	4.653
400	18250	2.602	4.261

Because the model is used only for the HCF region, the data considered in the analysis pertains to that region. The output of the regression analysis is provided in Table 18.

Table 18 Summary of regression analysis

	Coef-ficients	*Standard Error*	*t Stat*	*P-value*	*Lower 95%*	*Upper 95%*	*Lower 95.0%*	*Upper 95.0%*
β	3.209	0.087	36.843	0.000	2.996	3.422	2.996	3.422
α	-0.148	0.017	-8.945	0.000	-0.188	-0.107	-0.188	-0.107

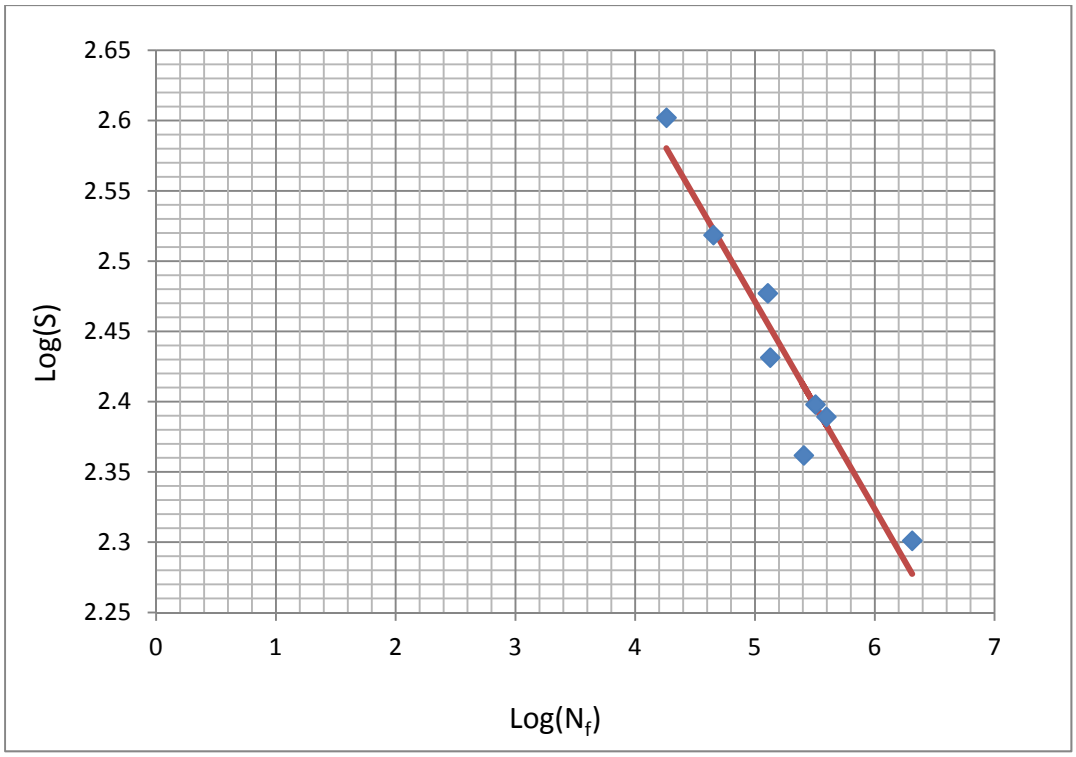

Fig.31 Log(N_f) variable line fit plot

The equation derived by regression analysis is:

$$\log S = -0.148 \log N_f + 3.21 \qquad (4.8)$$

So $\alpha = -0.148$ and $\beta = 3.21$

Now eq. (4.5) can be rewritten in a power law form:

$$S = 10^{\beta}(N_f)^{\alpha} \qquad (4.9)$$

Where $10^{\beta} = A$ and $\alpha = n$ are the required parameters for the power law model.

Substituting α and β we get the final model:

$$S = 10^{3.21}(N_f)^{-0.148} \qquad (4.10)$$

The resulted model Eq.4.10 is plotted in Fig.32 and compared to experimental data.

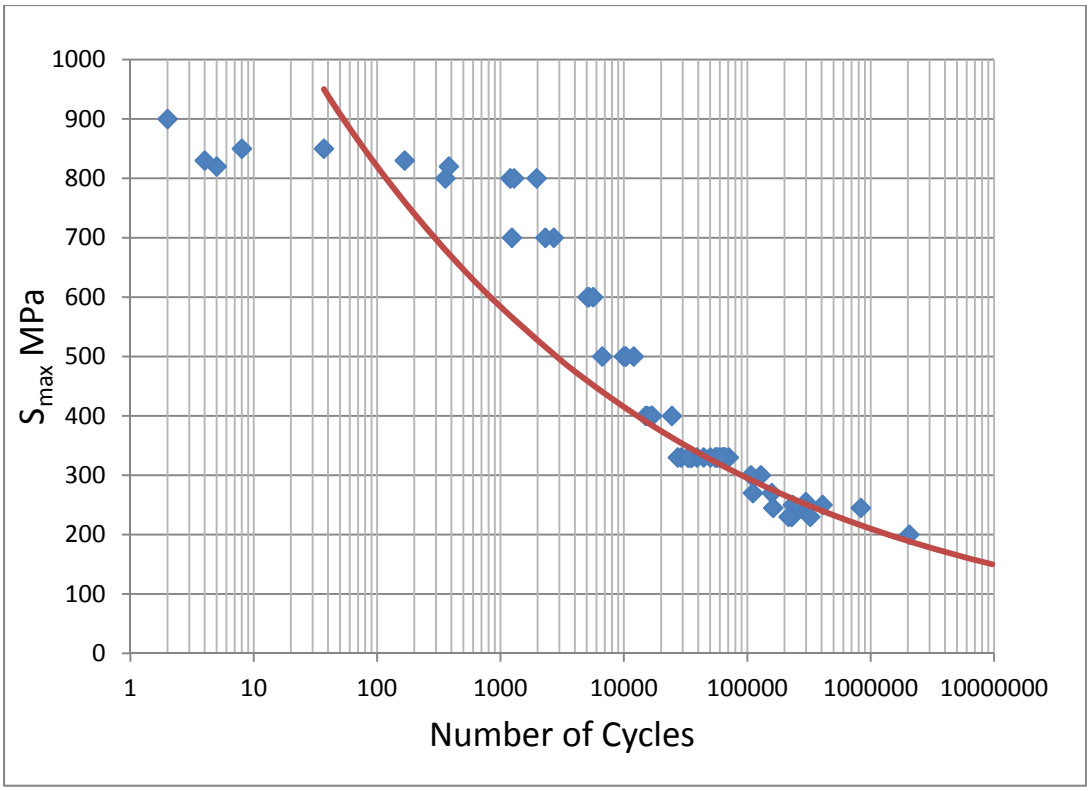

Fig.32 Power law model prediction compared to experimental data

Fig.32 clearly shows that the model agrees very well with tendency of the test data on the HCF region but mismatches behavior of the material in the LCF region. The reason is that at the stress level around 500 MPa and higher, the failure mode starts its transformation from tensile to compressive failure. That initiation was indicated in Fig.29. So the power law model is applicable for HCF region but it cannot be used for the LSF region. In the Fig. 33 the both compressive and tensile prediction models are plotted and compared to the experimental fatigue data. Unlike the power model, the Slaughter's model agrees quite well with experimental data in the LCF region dominated by compressive failure mode.

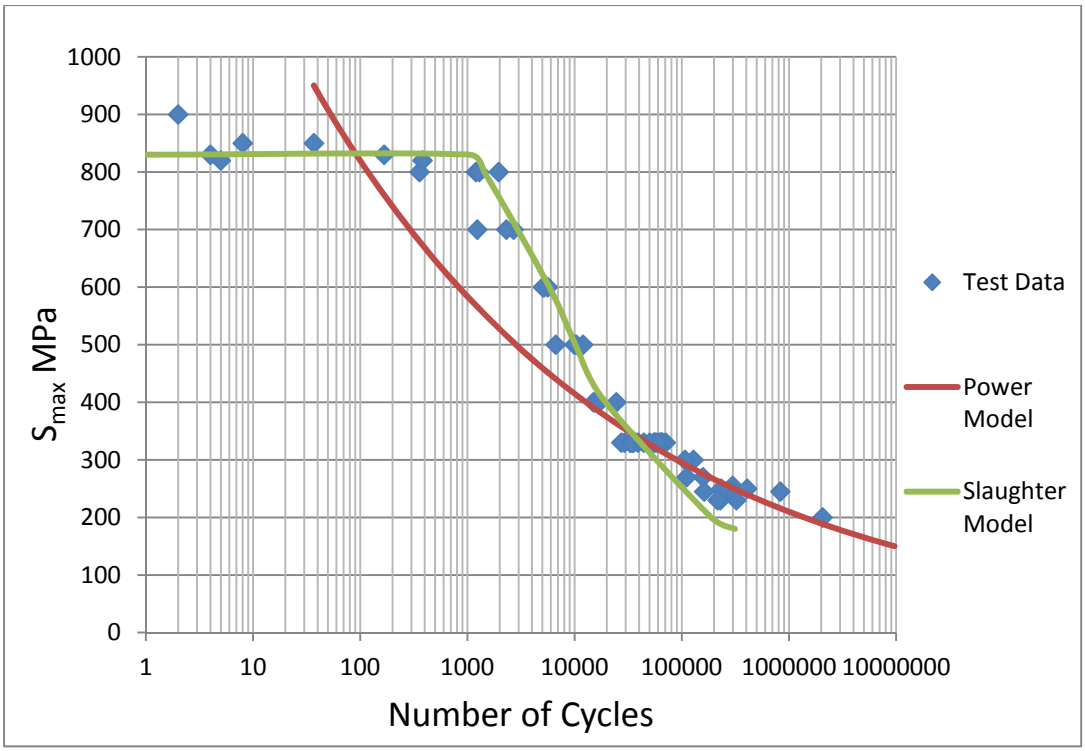

Fig.33 Slaughter's model#3 combined with power law model prediction

4.5 Test Results of the Frequency Effect

In order to evaluate the effect of frequency we ran 19 tests at a maximum stress of 330 MPa and $R = 0.1$. Samples were divided into three groups. The first group was tested at 6 Hz, the second at 8 Hz and the third at 10 Hz test frequency. All the tests were run in random order to minimize any other external influence. The results of the experiments were analyzed using the one-way ANOVA statistical tool. Table 19 lists the results of frequency testing.

Table 19 Fatigue test results of frequency testing

Specimen Number	Applied Stress (MPa)	Number of cycles to failure	Test Frequency (Hz)
CoFL 9	330	64250	8
CoFL57	330	63498	6
CoFL41	330	32994	10
CoFL37	330	29187	8
CoFL50	330	54944	10
CoFL31	330	27306	6
CoFL34	330	33294	8

Table 19 (Cont.)

CoFL35	330	44250	8
CoFL52	330	56134	10
CoFL 3	330	70737	8
CoFL40	330	35006	10
CoFL59	330	63000	6
CoFL27	330	34491	10
CoFL47	330	63995	8
CoFL44	330	66097	8
CoFL58	330	50168	6
CoFL46	330	60000	8
CoFL51	330	57432	10
CoFL30	330	39093	8
CoFL42	330	35579	6

4.6 ANOVA analysis

One-way analysis of variance (ANOVA) is a procedure of comparing sample means of a variable with each other and finding whether the results of variations are significantly different between each other [41]. The independent variable manipulated during the test was the test frequency. It consisted of three levels: 6 Hz, 8 Hz, and 10 Hz. The goal was to measure the mean fatigue lives resulted at each frequency level and compare their mean values between each other in order to determine if there is a difference in fatigue lives depending on the test frequency.

Table 20 presents the results of experiments, i.e. fatigue lives at 330 MPa stress level, separated into three groups according to frequency of a test.

Table 20 Fatigue life results for different test frequencies

Test Frequency	Number of Cycles to Failure							
6 Hz	63498	50168	63000	36000	27306			
8 Hz	33294	44250	63995	29187	70000	64250	66097	60000
10 Hz	34500	35000	54944	57432	56134	39093		

A one-way ANOVA was conducted on this data using MS Excel with 95% confidence level. The average of each group and the variance is shown below in output Tables 21 and 22.

Table 21 Summary of ANOVA analysis from MS Excel

Anova: Single Factor

Groups	*Count*	*Sum*	*Average*	*Variance*
6 Hz	5	239972	47994	2.61E+08
8 Hz	8	431073	53884	2.55E+08
10 Hz	6	277103	46184	1.23E+08

Table 22 Results of ANOVA analysis from MS Excel

ANOVA

Source of Variation	*SS*	*df*	*MS*	*F*	*P-value*	*F crit*
Between Groups	2.28E+08	2	1.14E+08	0.530	0.598	3.637
Within Groups	3.44E+09	16	2.15E+08			
Total	3.67E+09	18				

The F-score and P-value of one-way ANOVA indicates whether the effect of the independent variable was significant. In other words the significant F-statistic would tell that the test frequency had a significant effect on fatigue life of the composite beams tested. The F-score 0.598 is much lower than F critical 3.697, and P-value 0.598 is much higher than 0.05 which suggests that results of changing the test frequency do not differ significantly between each other, i.e. the range of test frequency that we dealt with does not affect the fatigue life of composite beams tested.

CHAPTER V

CONCLUSIONS AND RECOMMENDATIONS

The purpose of this study was to analyze the fatigue behavior of fiber-reinforced composite beams. The material used in the study was E-glass fibers in a polyester resin matrix. The material was supplied by LM Wind Power Company. The beams were tested under fatigue load at stress levels from 20% to 100% of the static failure stress of the material. All the tests were performed under load control conditions with sinusoidal loading with load ratio R=0.1. There was some four-point bending test data published on composite I beams, where one flange of the beam was carrying compressive loads and another a tensile load [34]. The design of the beam allowed analyzing each flange as a separate structure carrying uniaxial load. We did not find data published for a beam with a continuous cross-section where stress varied through the thickness of the beam.

The first step was to determine uniaxial and flexural properties of the composite material under static loading. Several problems related to the test coupon manufacturing, ply stacking, selecting size of the materials, etc were addressed. The first batch of test samples was made by hand lay-up method but poor consistency in properties of material from plate to plate was found. The decision was made to make plates using the VARTM process which achieved desirable quality of the material for testing. The high strength of the material and limitations on force capacity of the test machine required that the cross-section area of test coupons remain as small as possible and still be in agreement with ASTM requirements [36]. Also, in order to avoid stress concentrations, steel tabs were bonded to test coupons. A bonding material was

required which would be able to carry high loads without a failure. Apparently the tab had to be made wider than coupon itself to prevent early failure of material on the sides; this prevented a reduction of the potential strength of the tested material. The best combination of sample size, tab material, adhesive and manufacturing methods of the test coupons were identified.

The second step was the fatigue tests. A special fixture to perform four-point bending according to the test standard [38] was fabricated. Initially, all the fatigue tests were supposed to be performed at 10 Hz test frequency. But increasing the load caused a loss of stability in the testing process. The specimens would start jumping, vibrating, moving aside, etc. The specimens appeared to achieve resonance with the load head and at some point the machine would just stop because of load limitations. Reducing the test frequency for high stress levels down to 2 Hz solved the problem of resonance but all samples could not be tested with 1-2 Hz frequencies. Low stresses would have long (over two million cycles) life and it would take several months to complete all the tests. An analysis of other study results of frequency effect on fatigue life of composite materials showed that the frequency range in the current work was unlikely to have an effect on test results [32, 40]. Also it was decided to run another set of tests with constant load but varied frequency to evaluate the influence of test frequency on the fatigue life of our spesimens. The test data was analysed using ANOVA statistical tool which showed that a change in a test frequency did not significantly influence the results.

The primary purpose of this study was to analyze the fatigue behavior of a composite beam. Depending on the stress level, the failure mode of the composite beam changed from tensile failure on tension side of the beam to compressive buckling failure on the compressive surface of the beam. The slope of the S-N curve at the start of the region of high cycle fatigue is significantly different from the slope in the low cycle fatigue

region. This phenomenon might be due to two completely different reasons. One possibility is that composite material itself has different slopes for uniaxial compressive and tensile loading. That is shown for some materials in the fatigue database of composite materials developed at Montana State University [42]. As the bending of the beam causes both compressive and tensile stresses through the thickness, it is obvious that during progressive increase or decrease of the stress level the material would fail differently depending on which type of resistance (compressive or tensile) is weaker at a given stress level. Another possible reason for the slope change might come from the fact that compressive loading itself, depending on the stress level, changes the failure mode from fatigue micro-buckling to monotonic micro-buckling. The" jump" of the fatigue at the stress level is related to transition from one mode to another and the point of transition is called by researchers as the plastic collapse point [25].

Most probably the change in slope of the S-N curve of the composite beam is not only the result of one of listed factors but combination of them. In order to have a better picture of processes that possibly happen in a beam we need to know the fatigue behavior of the material under uniaxial compression and tension. Considering those slopes we can possibly transfer them to case of the beam. In this particular case, we did not have a chance to test the material under uniaxial fatigue loading because of load limitations of the fatigue machine. For example, the static failure load of tensile specimens was about 25 kN, whereas the maximum load capacity of our fatigue testing machine is only 7.5 kN. Knowledge of the uniaxial fatigue properties of this material would open another possible direction of research for this type of materials. While looking for bending fatigue test data for composite materials, no published data for fully-reversed (R=-1) fatigue was found. The behavior of the beam is expected to be absolutely different under fully-reversed fatigue loading. Each surface of the beam would

experience compressive micro-buckling and tensile opening damage at the same time. So the speed of the damage might increase incredibly or decrease as it happens with some solid materials during compressive fatigue (crack closure phenomenon). Initially, it was planned to do fully reversed fatigue tests, but a fixture was not available to constrain the beam properly. The current fixture would tightly fix the supporting end, creating unwanted bending moments on the ends of the beam. One possible solution is to use special fixtures on rollers, which would securely fix the beam in vertical direction (i.e. direction of applied load) and let the ends of the beam rotate freely.

Further uniaxial fatigue and fully reversed bending fatigue tests are needed to have a fuller picture of the fatigue performance of this material.

REFERENCES

1. Schulte K., Reese E., Chou T. W. (1987) Fatigue Behavior and Damage Development in Woven Fabric and Hybrid Composites. In: Matthews F.L., Buskell N.C.R., Hodgkinson J.M., and Morton J. Six International Conference on Composite Matrerials (ECCM-II), Volume 4, Proceedings 20-24 July, 1987, London, UK, Elsevier pp. 4.89-4.99.
2. Chen A.S. Matthews F.L. (1993) Biaxial Flexural Fatigue of Composite Plates. In: Miravete A. editors ICCM/9 Composites: Properties and Aplications, Proceedings of Ninth International Conference on Composite Materials, vol VI. Woodhead Publishing Limited, Madrid, Spain.
3. Degrieck J., Van Paepegem W. (2001). Fatigue Damage Modeling of Fiber-Reinforced Composite Materials. Department of Mechanical Construction and Production, Ghent University, Sint-Pietersnieuwstraat 41,9000 Gent, Belgium.
4. Hashin Z., Rotem A., (1973). A fatigue criterion for fiber reinforced Composite Materials. J Composite Mat., 7,448-464
5. Fawaz Z., and Ellyin F., (1994). Fatigue Failure Model for Fiber-Reinforced Materials under the General Loading Conditions. J Composite Mat., 28(15), 1432-1451.
6. Bond I. P. (1999). Fatigue Life Prediction for GRP Subjected to Variable Amplitude Loading. Composites, Part A, Applied Science and Manufacturing 30(8), 961-970.
7. Xiao X.R. (1999). Modeling of Load Frequency Effect on Fatigue Life of Thermoplastic Composites. J Composite Mat., 33, 1141-1158.
8. Hwang W. and Han K.S. (1986b). Fatigue of Composites Fatigue Modulus Concept and Life Prediction. J Composite Mat., 20,154-165.
9. Van Paepegem W. and Degrieck J. (2000). Numerical Modeling of Fatigue Degradation of Fiber-Reinforced Composite Materials. Proceeding on Fifth International Conference on Computational Structures Technology, Volume F: Computational Technics For Materials, Composites and Composite Structures, Leuven, 6-8 September, 2000, Civil Comp. Press., pp. 319-326.
10. Sidoroff F. and Subagio B. (1987). Fatigue Damage Modeling of Composite Materials from Bending Tests. In: Matthews F.L., Buskell N.C.R., Hodgkinson J.M., and Morton J. Six International Conference on Composite Matrerials (ECCM-II), Volume 4, Proceedings 20-24 July, 1987, London, UK, Elsevier pp. 4.32-4.39.
11. Chou P.C. and Croman R. (1979). Degradation and Sudden Death Models of Fatigue of graphite/epoxy composites. In: Tsai S.W. Composite Materials:

Testing and Design (Fifth Conference), ASTM STP 64, Philadelphia, American Society for Testing and Materials, pp.431-454.
12. Hahn H.T. and Kim R.Y. (1975). Proof Testing of Composite Materials. J Composite Materials. 9, 297-311.
13. Sendeckyj G.P. (1981). Fitting Models to Composite Material Fatigue Data. In: Chamis C.C. Test Methods and Design Allowables for Fibrous Composites. ASTM STP 734, American Society for Testing and Materials, pp.245-260.
14. Halpin J. C., Jerina K. L., Johnson T. A. (1973). Characterization of Composites for the Purpose of Reliability Evaluation. In: Analysis of the Test Methods for High Modulus Fibers and Composites. ASTM ASP 521, pp.5-64.
15. Rotem A. (1986). Fatigue and Residual Strength of Composite Laminates. Engineering Fracture Mechanics, 25, 819-827
16. Rotem A. (1991). Fatigue Bahavior of Composite Laminates under Various Mean Stresses. Composite Structure, 17, pp.113-126.
17. Caprino G. and D'Amore A. (1998). Flexural Fatigue Behavior of Random Continuous-Fiber-Reinforced Thermoplastic Composites, Composites Sci. Tech. 58, 957-965.
18. Caprino G. (2000). Predicting Fatigue Life of Composite Laminates Subjected to Tension-Tension Fatigue. J Composite Mat. 34, 1334-1335.
19. Biner S. B. and Yuhas V. C. (1989). Growth of Short Fatigue Cracks at Notches in Woven Fiber Glass Reinforced Polymeric Composites, J Eng. Mat. Tech. 111, 363-367.
20. Dahlen C. and Springer G. S. Delamination Growth in Composites under Cyclic Loads, J Composite Mat 28, 732-781.
21. Feng X., Gilchrist M. D., Kinloch A. J., and Matthews F. L. (1997). Development of a Method for Predicting The Fatigue Life of CFRP Components. In: Degallaix S., Bathias C., and Fougeres R. (eds.), International Conference on Fatigue of Composites. Proceedings, 3-5 June, 1997, Paris, France, La Societe Francaise de Metallurgie et de Materiaux, pp. 378-385.
22. Ogin S. L., Smith P.A., Beaumont P.W.R. (1985). Matrix Cracking and Stiffness Reduction During the Fatigue of $(0/90)_s$ GFRP Laminate. Composites Sci. Tech. 22(1) pp. 23-31.
23. Carswell W.S. (1988). Damage Mechanics of Composite Behavior Composite Structures, 10,335-342
24. Caron J. F. and Ehrlacher A. (1997). Modelling of Fatigue Microcracking Kinetics in Cross ply and Experimental Validation. In: Degallaix S., Bathias C., and Fougeres R. (eds.), International Conference on Fatigue of Composites. Proceedings, 3-5 June, 1997, Paris, France, La Societe Francaise de Metallurgie et de Materiaux, pp.378-385.
25. Slaughter W.S. and Fleck N.A. (1993). Compressive Fatigue of Fiber Composites. Campridge University, Engineering Department, Cambridge, CB2 1 PZ, U.K.

26. Budiansky B. and Fleck N.A. (1993). Compressive Failure of Fiber Composites. J Mech. Phys. Solids. 41, pp.138-211.
27. Nijssen R., Cormier L. (2010) Experiments and Modeling of of Influence and Interaction of Temperature and Test Frequency on Fatigue Life. Knowledge Center Wind Turbine Materials and Constractions. Wieringerwerf, Netherlands.
28. Creed R. F.(19930 High Cycle Tensile Fatigue of Unidirectional Fiberglass Composite Tested at High Frequency. M.S. Thesis, Department of Chemical Engineering, Bozeman, Montana.
29. Beaumont P.W.R. The Mechanics of Fatigue Damage in Structural Composite Materials. In: Fuller J., Gruninger G., Schulte K., Bunsell A.R., and Massiah A. (eds.) Developments in Science and Technology of Composite Materials, Proceedings of the Fourth European Conference on Composite Materials (ECCM/4), 25-28 September, 1990, Stuttgart, Elsevier Applied Science, pp.195-205.
30. Mandel J.F. and Meier U. (1983). Effect of Stress Ratio Frequency and Loading Time on the tensile Fatigue of Glass reinforced Epoxy In: Long Term Behavior of Composites ASTM STP 813 O'Brain T.K. ed. America Society of Testing and Materials, pp. 55-77.
31. ISO 13003:2003 Fiber-Reinforced Plastics-Determination of Fatigue Properties under Cyclic Loading Conditions
32. McCrum N.G., Buckley C.P., and Bucknal C.B.(1988). Principles of Polymer Engineering, Oxford University Press, New York.
33. Mandel J.F. (1991). Fatigue Behavior of Short Fiber Composites Materials in Fatigue of Composite Materials, Reifsnider K.L. Elsevier Science Publishers, New York, pp. 232-233.
34. Samborsky, Daniel D.(1999). Fatigue of E-glass Fiber Reinforced Composite Materials and Substructures. M.S. Thesis, Department of Civil Engineering, Montana State University.
35. Daniel i.m., Ishai O. (2006). Engineering Mechanics of Composite Mechanics Oxford University Press, New York.
36. ASTM D3039 / D3039M - 08 Standard Test Method for Tensile Properties of Polymer Matrix Composite Materials. Annual Book for ASTM Standards. Vol.15.03 pp.106-118.
37. ASTM D3171 Standard Test Method for Constituent Content of Composite Materials. Annual Book for ASTM Standards. Vol.15.03
38. ASTM D6272 – 08 Standard Test Method for Flexural Properties of Unreinforced and Reinforced Plastics and Electrical Insulating Materials by Four-Point Bending. Annual Book for ASTM Standards. Vol.08.03 pp.106-118.
39. Theory Reference for the Mechanical APDL and Mechanic Applications. SOLID 185 Homogeneous Structural Solid Element Descriptions. ANSYS Release 13.0 SAS IP, Inc. 2010
40. Huang, Y.H. and Wang S.S. (1989) Compressive Fatigue damage and associated property degradation of aluminum-matrix composite. Proc 4th Japan, US conference of composite materials, 27-29 June, 1988, Washington D.C., Technomic, WestPoert, CT. pp.606-632.

41. Lawson J. S. and Erjavec J. Modern Statistics for Engineering and Quality Improvement. Duxbury Press. 1st Edition December, 2000.
42. DOE/MSU Composite Material Fatigue Database, Version 19.0 March 31, 2010